Evaluation of the accuracy of thermal dissociation CRDS and LIF techniques for atmospheric measurement of reactive nitrogen species

Caroline C. Womack[1], J. Andrew Neuman[1,2], Patrick R. Veres[1,2], Scott J. Eilerman[1,2], Charles A. Brock[1], Zachary C. J. Decker[3], Kyle J. Zarzana[1,2], William P. Dube[1,2], Robert J. Wild[1,2], Paul J. Wooldridge[4], Ronald C. Cohen[4,5], Steven S. Brown[1,3]

[1]Chemical Sciences Division, Earth Science Research Laboratory, National Oceanic and Atmospheric Administration, Boulder, CO 80305 USA
[2]Cooperative Institute for Research in Environmental Sciences, University of Colorado, Boulder, CO 80309 USA
[3]Department of Chemistry and Biochemistry, University of Colorado, Boulder, CO 80309 USA
[4]Department of Chemistry, University of California, Berkeley, CA 94720 USA
[5]Department of Earth and Planetary Science, University of California, Berkeley, CA 94720USA

Correspondence to: S. S. Brown (steven.s.brown@noaa.gov)

Abstract. The sum of all reactive nitrogen species (NO_y) includes NO_x (NO_2 + NO) and all of its oxidized forms, and the accurate detection of NO_y is critical to understanding atmospheric nitrogen chemistry. Thermal dissociation (TD) inlets, which convert NO_y to NO_2 followed by NO_2 detection, are frequently used in conjunction with techniques such as laser induced fluorescence (LIF) and cavity ringdown spectroscopy (CRDS) to measure total NO_y when set at >600 °C, or speciated NO_y when set at intermediate temperatures. We report the conversion efficiency of known amounts of several representative NO_y species to NO_2 in our TD-CRDS instrument, under a variety of experimental conditions. We find that the conversion efficiency of HNO_3 is highly sensitive to the flow rate and the residence time through the TD inlet, as well as the presence of other species that may be present during ambient sampling, such as ozone (O_3). Conversion of HNO_3 at 400 °C, nominally the set point used to selectively convert organic nitrates, can range from 2-6% and may represent an interference in measurement of organic nitrates under some conditions. The conversion efficiency is strongly dependent on the operating characteristics of individual quartz ovens, and should be well calibrated prior to use in field sampling. We demonstrate quantitative conversion of both gas phase N_2O_5 and particulate ammonium nitrate in the TD inlet at 650 °C, the temperature normally used for conversion of HNO_3. N_2O_5 has two thermal dissociation steps, one at low temperature representing dissociation to NO_2 and NO_3, and one at high temperature representing dissociation of NO_3, which produces exclusively NO_2 and not NO. We also find a significant interference from partial conversion (5-10%) of NH_3 to NO at 650 °C in the presence of representative (50 ppbv) levels of O_3 in dry zero air. Although this interference appears to be suppressed when sampling ambient air, we nevertheless recommend regular characterization of this

interference using standard additions of NH_3 to TD instruments that convert reactive nitrogen to NO or NO_2.

1 Introduction

The catalytic cycling of nitrogen oxides (NO_x = NO + NO_2) plays a key role in the formation of tropospheric ozone (O_3) from the photooxidation of VOCs. Reactive nitrogen species, such as alkyl and multifunctional nitrates (ANs, $RONO_2$), peroxy nitrates (PNs, RO_2NO_2) and nitric acid (HNO_3) serve as reservoirs and sinks of NO_x. The formation of these species results in chain termination that determines the efficiency of the O_3 production cycle, and can also transport NO_x far from the original emission source. For this reason, total reactive nitrogen (NO_y = NO + NO_2 + $RONO_2$ + RO_2NO_2 + HNO_3 + HONO + NO_3 + 2 × N_2O_5 + aerosol nitrates) is an important tracer in monitoring tropospheric O_3 production. Its accurate detection is critical in field measurements of ambient air quality, as O_3 is a known health risk, and a number of regions across the US are currently in non-attainment or near non-attainment with national ambient air quality O_3 standards (EPA, 2016). However, the sources and fates of NO_y species are complex and remain poorly characterized in some regions. Measured total reactive nitrogen has in some cases deviated significantly from the sum of the measured individual components, $\Sigma NO_{y,i}$ (see (Fahey et al., 1986;Bradshaw et al., 1998;Neuman et al., 2012) and others referenced within). This unmeasured NO_y, sometimes referred to as "missing NO_y", indicates the need for a more complete understanding of total and speciated reactive nitrogen, and for accurate analytical instrumentation for NO_y measurement (Crosley, 1996;Williams et al., 1998;Day et al., 2003).

Techniques that detect the major individual components of NO_y include detection of NO and NO_2 by chemiluminescence (Ridley and Howlett, 1974;Kley and McFarland, 1980), cavity ringdown spectroscopy (CRDS) (Fuchs et al., 2009), or laser induced fluorescence (Thornton et al., 2000), and detection of HNO_3 by chemical ionization mass spectrometry (CIMS) (Fehsenfeld et al., 1998;Huey et al., 1998;Neuman et al., 2002;Huey, 2007) or mist chamber sampling (Talbot et al., 1990). Additionally, speciated peroxy acetyl nitrates (PANs) have been detected by gas-chromatography electron capture detection (Darley et al., 1963;Flocke et al., 2005) and CIMS (Slusher et al., 2004), while N_2O_5 and $ClNO_2$ have been detected by CRDS (Dubé et al., 2006;Thaler et al., 2011) and CIMS (Kercher et al., 2009). HONO has been detected by long path differential optical absorption spectroscopy (Perner and Platt, 1979) and NO_3 has been detected by CRDS (King et al., 2000). However, fewer methods have been developed for detection of the broad suite of individual alkyl and multifunctional nitrates, which have been suggested to comprise upwards of 20% of NO_y in the midlatitude continental boundary layer and may be higher in remote locations (O'Brien et al., 1995;Day et al., 2003;Worton et al., 2008;Beaver et al.,

2012;Xiong et al., 2015;Lee et al., 2016). An alternative to detecting individual components of NO_y is the use of a molybdenum oxide or gold catalyst in the presence of CO to reduce all NO_y species to NO, followed by NO detection by chemiluminescence (Winer et al., 1974;Fahey et al., 1986), though catalyst-based techniques are known to require frequent cleaning, and are potentially sensitive to contamination and to interferences at ambient levels of ammonia, HCN, acetonitrile, and R-NO_2 compounds (Crosley, 1996;Kliner et al., 1997;Bradshaw et al., 1998;Williams et al., 1998;Day et al., 2002). An alternative method developed by Day and co-workers (Day et al., 2002) uses a quartz thermal dissociation (TD) inlet to rapidly thermally convert nearly all NO_y species to NO_2, which is then detected by laser induced fluorescence (LIF). The NO_y species in the TD inlet undergo the following reaction

$$XNO_2 + \text{heat} \rightarrow X + NO_2 \quad (1)$$

where X is HO, RO, or RO_2. Heated inlets had previously been used to dissociate PNs (Nikitas et al., 1997), but the TD inlet developed by Day et al. (2002) takes advantage of the different O-N bond energies of ANs, PNs, and nitric acid to separately and selectively detect these three classes of NO_y. A plot of measured NO_2 signal as a function of inlet temperature (hereafter referred to as a "thermogram") yields a stepwise dissociation curve with increases in signal near 100, 300 and 500 °C, corresponding to the dissociation of PNs, ANs, and HNO_3 respectively. By setting the TD oven temperature to one of the three plateaus, they were able to measure each class of NO_y, by comparison of the NO_2 signal in a given channel to the signal measured at the adjacent lower temperature plateau.

In recent years, a suite of other instruments have incorporated this NO_y TD inlet method into existing techniques that measure NO_2 or the radical cofragment X in Eq. (1), such as chemical ionization mass spectrometry (TD-CIMS) (Slusher et al., 2004;Zheng et al., 2011;Phillips et al., 2013), cavity ringdown spectroscopy (TD-CRDS) (Paul et al., 2009;Thieser et al., 2016), and cavity attenuated phase shift spectroscopy (TD-CAPS) (Sadanaga et al., 2016). Each instrument has its own advantages and disadvantages. For example, TD-LIF detects NO_2 at low pressure following thermal dissociation. Secondary recombination reactions of the dissociated radicals would thus be suppressed in the detection region, although the thermal dissociation inlet may be operated at either high or low pressures in these instruments. However, it is subject to interferences from urban levels of NO and NO_2 (Paul et al., 2009;Wooldridge et al., 2010). TD-CIMS can differentiate between the different types of PNs, but requires regular calibration of each species, not all of which have native standards readily available. TD-CAPS is subject to interferences from glyoxal and methylglyoxal (Sadanaga et al., 2016). TD-CRDS is an absolute measurement, but can be subject to other interferences, as discussed in Sect. 3.

Recent TD inlet studies (Day et al., 2002;Paul et al., 2009;Thieser et al., 2016) have measured the conversion efficiency for several AN and PN species with known concentrations in a laboratory setting. These studies all note the possibility of secondary reactions that either increase or decrease the NO_2 signal. For example, recombination reactions to reform the AN or PN species prior to reaching the detector will result in a negative bias in NO_2 (too little NO_2 measured). Likewise, ambient levels of O_3 in the sampled air may react in the oven with NO to form NO_2, resulting in a positive bias (Pérez et al., 2007), though this reaction rate depends on the TD inlet pressure and flow rate (Wooldridge et al., 2010). Day et al. (2002) found that recombination reactions were significant for PNs, but caused minimal problems for nitric acid, since the OH radical is far more likely to be lost to the walls of the oven than to recombine with NO_2. More significant is the reaction of dissociated RO_2 and HO_2 radicals with ambient levels of NO and NO_2. Thieser et al. (2016) parameterized the bias in peroxyacetyl nitrate and 2-propyl nitrate detection in their inlet as a function of ambient NO and NO_2 concentrations, but noted that these parameterizations may vary for other PNs or ANs. In cases where the concentration of one category of NO_y species far exceeds the others, such as the high HNO_3:ANs ratios in Pusede et al. (2016), speciated measurements can be significantly affected by biases in measurements of the other NO_y compounds.

A four-channel CRDS instrument (hereby referred to as the NOAA TD-CRDS instrument) for detection of nitrogen oxides was recently developed (Wild et al., 2014). In this instrument, one channel is equipped with a TD inlet set at 650 °C and is used to measure all NO_y species (including NO_2, and NO by chemical conversion with an O_3 addition to NO_2). Two other channels simultaneously monitor NO_2 and NO, and so a measurement of NO_z (= NO_y – NO_x) can be derived. Because NO is intentionally detected as NO_2 in the NO_y channel, this instrument avoids the majority of the NO ↔ NO_2 interconversion interferences that affect many other thermal dissociation instruments. Analogous to the studies which measured the conversion efficiencies of ANs and PNs (Day et al., 2002;Paul et al., 2009;Sadanaga et al., 2016;Thieser et al., 2016), we present here an analysis of the conversion efficiencies of several other NO_y species, and the interferences that affect the operation of this high temperature inlet. These interferences include the temperature dependence of HNO_3 conversion, which is important to understanding both its quantitative conversion at 650°C as well as its potential to interfere with measurements of ANs at lower temperatures. We also compare these results to those from the TD-LIF instrument of Day et al. (2002), hereby referred to as the Berkeley TD-LIF instrument. Additionally, we report the temperature dependence of N_2O_5 conversion, which is shown to occur in two steps, the conversion efficiency of ammonium nitrate aerosol, and finally the interference of NH_3 through its partial conversion to NO.

2 Methods

2.1 Thermal dissociation cavity ringdown spectroscopy (TD-CRDS)

Cavity ringdown spectroscopy is a direct absorption technique for measuring the concentration of trace gases (O'Keefe and Deacon, 1988;Fuchs et al., 2009). The four-channel 405 nm NOAA TD-CRDS instrument, which has been used by our group in both lab-based studies and atmospheric sampling (Wild et al., 2014;Wild et al., 2016), simultaneously measures ambient NO_2 in one channel, while chemically converting NO and O_3 to NO_2 in the second and third channels, and thermally converting NO_y to NO_2 in a TD oven in the fourth channel. In this study, we have used only the NO_y channel to study the conversion efficiency of several reactive nitrogen species to NO_2. Figure 1 shows a schematic of the relevant instrument plumbing and optical cavity. The details of the optical cavity can be found in (Wild et al., 2014); only a brief description of the optical system and the details of the TD inlet that deviate from that study will be described here.

Sampled air is pulled into a 50 cm long high-finesse optical cavity capped by highly reflective end mirrors, with purge flows of 25 sccm (cubic centimeters per minute at 273.15 K and 1 atm) added in front of each mirror to maintain mirror cleanliness. The output of a 0.5 nm bandwidth, continuous wave diode laser centered at approximately 405 nm and modulated at 2 kHz is passively coupled into one end of the optical cavity. The laser light builds up in the cavity, and when it is modulated off, the decaying output light intensity is monitored by photomultiplier tube on the far side of the cavity. The measured light decay profiles are summed and fit at a 1 Hz repetition rate to yield the ringdown time τ. The ringdown time is inversely related to the concentration of the absorbing gas, NO_2 in this case, which can be derived as

$$[NO_2] = \frac{R_L}{c\sigma}\left(\frac{1}{\tau} - \frac{1}{\tau_0}\right) \quad (2)$$

where R_L is the ratio of d, the mirror separation length, and l, the distance over which the sample is present. The speed of light is represented by c, σ is the absorption cross section of NO_2, and τ_0 is the ringdown time of a reference cavity without any absorbing gases, which is obtained by flushing the cavity with an excess flow of zero air for 30 seconds every 10 to 20 minutes. If purge volumes were not used, the R_L term in Eq. (2) would simply be 1, but since purge volumes are used here, σ/R_L is characterized regularly by filling the cavity with several different known NO_2 concentrations (obtained by reacting the output of an O_3 standard source with excess NO) and calculating the slope of the measured optical extinction vs [NO_2] as described in Washenfelder et al. (2011). This value was measured approximately once per month during laboratory tests with this instrument, but was constant to within ±1%, with an

average value of 6.25×10^{-19} cm^2. More regular calibrations of the σ/R_L value during recent field studies show similar stability. The NO_2 signal can be measured with a lower detection of 18 pptv (1σ) in 1 second (Wild et al., 2014).

The NO_y TD oven inlet consists of a quartz tube (0.39 cm ID, 63 cm in length, 38 cm of which is heated) wrapped in Nichrome wire and insulated with fiberglass. The flow rate through the inlet and optical cavity is controlled by a mass flow controller on the downstream side of the optical cavity. Because the standard flow rate is held constant during each experiment, the volumetric flow rate, and therefore the TD residence time, varies with oven temperature. For example, the 4.5 cm^3 inner volume of the oven results in an oven residence time of 30 - 100 ms at a flow rate of 1.9 slpm (slpm = liters per minute at 273.15 K and 1 atm) for temperatures from 25 – 650 °C. 1.9 slpm represents the normal operating conditions of this instrument, but flow rates between 0.25 and 3 slpm were tested, which provides oven residence times between 20 and 400 ms. The temperature of the TD oven is monitored by a thermocouple mounted to the outer side of the quartz tube, and therefore is slightly lower than the temperature of the gas. However, inserting a temperature probe into the inner part of the TD inlet yields a temperature profile, shown in Fig. S1, which approaches the temperature set point by the end of the inlet. All oven temperatures described hereafter refer to the measured thermocouple temperature. After passing through the TD oven, the gas cools to room temperature in the non-heated portion of the quartz tube, passes through a particle filter (47 mm diameter, 1 μm pore size PTFE membrane) to remove non-volatilized particles, and then enters a 15 cm^3 mixing volume prior to entering the CRDS cavity. There, O_3 (~30 ppmv after dilution) is added to the sampled air to convert any NO that formed in the thermal dissociation to NO_2. As the rate constant for the $NO + O_3 \rightarrow NO_2 + O_2$ reaction is more than three orders of magnitude faster than the $NO_2 + O_3 \rightarrow NO_3 + O_2$ reaction, conversion of NO_2 to NO_3 (and subsequently to N_2O_5) is at most 1-2% in this mixing volume and is corrected for using a previously described method (Fuchs et al., 2009). To measure the thermograms shown in this paper, the oven temperature was set to a sequence of temperatures spanning 300 to 650 °C and spaced by 25 °C in a random order. The measured NO_2 concentrations are averaged at each temperature set point for approximately 10 – 15 minutes.

2.2 NO_y samples and additions

Samples of reactive nitrogen species (labeled as "NO_y source" in Fig. 1) were introduced into the TD oven in several ways. HNO_3 and NH_3 were obtained by passing a 50 sccm flow of zero air through a calibrated 45 °C permeation tube containing HNO_3 (VICI Metronics) or NH_3 (KinTek), providing gaseous outputs of 64 and 23 ng/min, respectively (Neuman et al., 2003). Subsequent dilution in 0.5 - 4 slpm zero (synthetic) air resulted in HNO_3 and NH_3 concentrations of 5 to 40 ppbv. Because both these

species readily adsorb to instrument surfaces (Neuman et al., 1999), only FEP Teflon tubing was used between the permeation tube and the TD oven, all tubing was kept as short as possible (typically less than 30 cm) and was wrapped in 100°C heating tape to reduce losses to the walls. However, these precautions were found to be unnecessary in this laboratory study, since the constant flow from the permeation tube resulted in an equilibrium in which the adsorption losses to the walls were equal to the rate of off-gassing.

NO was obtained by dilution of the output of a calibrated standard (Scott-Marrin, 0.2% in N_2). N_2O_5 was synthesized via a procedure adapted from Davidson et al. (1978) and Bertram et al. (2009), which has been used as a calibration for the N_2O_5 channel of a CRDS NO_3 instrument (Dubé et al., 2006;Wagner et al., 2011). Pure samples of NO and O_2 were mixed to yield NO_2, and this mixture was reacted in a flow tube with excess O_3, yielding NO_3 which then reacted with NO_2 to form N_2O_5. The resulting mixture flowed through a glass trap at -78°C, where N_2O_5 solidified as a white crystal. A gaseous sample of N_2O_5 was obtained by flowing 20 - 50 sccm of zero air over the solid -78 °C sample, and then diluting further in zero air. Gas phase N_2O_5 prepared in this way is known to contain variable but significant amounts of HNO_3 (Bertram et al., 2009), and thus efforts were made to minimize this interference by baking all glassware for several hours before use, and by distilling the solid N_2O_5 sample regularly by bringing it to room temperature under an O_3 flow for 10 minutes. Nevertheless, some HNO_3 was always present in the sample, and therefore the output of the trap was passed through a nylon wool scrubber prior to entering the TD oven, which removed HNO_3 without significantly perturbing the N_2O_5 concentration. Finally, ammonium nitrate particles were generated by running a 0.1 g/L solution of aqueous NH_4NO_3 through an atomizer and size-selecting particles of a certain diameter with a custom-built differential mobility analyzer (DMA). Conductive tubing, rather than Teflon, was used to minimize electrostatic build up and loss of particles to the walls before entering the TD oven.

In order to test whether common atmospheric gases would interfere with the conversion efficiency, some additional species were added to the sample prior to entering the oven. Water was added by passing the dilution zero air through a water bubbler prior to mixing with the HNO_3 sample. Various amounts of O_3 were added by running the dilution zero air through an O_3 calibrator (Thermo Scientific 49i) that is also capable of generating up to 200 ppm O_3 in 1 - 3 slpm of zero air. We also investigated the effect of various VOCs, including a high concentration of propane (~5 ppmv) and a standard mixture of VOCs (Air Liquide) consisting of n-hexane (1.234 ppm), propanal (0.397 ppm), 2-butanone (1.237), benzene (1.151 ppm), methylcyclohexane (0.938 ppm), ethylbenzene (1.213 ppm), 2,2,4-trimethylpentane (1.186 ppm), isopropyl benzene (1.148 ppm) and ethanol (0.994 ppm). This mixture is commonly used to calibrate GC/MS instruments, but here provides common atmospheric species with a range of masses, bond strengths, and degrees of oxidation. It was diluted to 50 ppbv total VOCs by addition of zero air prior to entering the oven. We also added CO in varying quantities to the HNO_3 and NH_3 samples.

2.3 Ancillary measurements

Several instruments were used as ancillary confirmation for some of the NO_y sample concentrations. In each case, a Teflon tee split the sample input and a portion of the flow was pulled into the secondary instrument prior to entering the TD oven, as shown in Fig. 1. In the case of NH_3, a Picarro G2103 NH_3 Analyzer with a manufacturer's specified 1 ppbv detection limit at 5 second integration time was used. A custom-built iodide adduct chemical ionization mass spectrometer (Lee et al., 2014), described in further detail in (Veres et al., 2015), was used to monitor the N_2O_5 and HNO_3 concentrations from the N_2O_5 solid sample prior to dissociation in the oven. In this instrument, N_2O_5 and HNO_3 mixed with I^- ions produced by passing CH_3I through a ^{210}Po source, and the resulting $HNO_3 \cdot I^-$ and $N_2O_5 \cdot I^-$ ions were detected by quadrupole mass spectrometry at m/z = 190 and 235. This measurement has a detection limit of 4 pptv and 70 pptv and error bars of 25% and 25% (3σ) for N_2O_5 and HNO_3, respectively. Lastly, an ultra-high sensitivity aerosol spectrometer (Droplet Measurement Technologies) was used to monitor the size distribution of the size-selected ammonium nitrate particles (Cai et al., 2008).

HNO_3 and NH_3 conversion efficiencies were also tested using ambient air for dilution (rather than synthetic air), as sampled during daytime in August 2016 in Boulder, CO. Ambient air was drawn into the two of the four channels of the NOAA TD-CRDS instrument, through two side-by-side identical quartz ovens heated to 650 °C at a flow rate of 1.4 slpm, and the output of either the NH_3 or HNO_3 permeation tube was inserted directly into the exposed inlet of one of the ovens, for a duration of approximately 6 minutes. The NO_2 signal was measured by one of the remaining channels in the NOAA TD-CRDS instrument, and the conversion efficiency of each species was calculated by comparing the difference in NO_2 signal between the two ovens relative to the calibrated output of the permeation tube, to correct for small differences in NO_2 signal between the two ovens.

We also present results measured in the Berkeley TD-LIF instrument. It is described in greater detail elsewhere (Day et al., 2002), but briefly, HNO_3 and *n*-propyl-nitrate samples were provided by permeation tubes similar to those described in Sect. 2.2, diluted in dry zero air, and passed through 20 cm heated length quartz ovens, held at ambient pressure, at a flow rate of 2 slpm. This resulted in residence times of approximately 50 ms. The NO_2 released in the thermal conversion was supersonically expanded into the detection region and measured by laser induced fluorescence from an individual ro-vibronic NO_2 line. The NO_y conversion ratio was calculated as the measured NO_2 concentration relative to the maximum NO_2 signal at high temperatures, as the oven temperature was changed at a rate of -10 ^oC per minute.

2.4 Box modeling

A simple kinetic box model was used to support the experimental findings. Reaction rates for ~60 reactions possibly involved in the dissociation and secondary chemical reactions of each NO_y species (listed in the Supporting Information), were obtained from the JPL Kinetics Database (Sander et al., 2011) and the NIST Chemical Kinetics Database (Manion et al., 2015) at temperatures spanning the 25 - 650 °C range of the experimental thermograms. For every HNO_3, N_2O_5, and NH_3 thermogram, a simulation was run at each temperature, assuming a starting concentration of the NO_y species equal to that observed in the experiment, and lasting the duration of the residence time in the oven. The simulation was then allowed to keep running at room temperature for an additional ~1 second to mimic the conditions between the oven and the instrument. During this additional low temperature time, 30 ppmv of O_3 was added to the simulation to convert NO to NO_2 as in the TD-CRDS instrument. The final concentration of NO_2 at the end of the simulation was recorded for each temperature, which resulted in a simulated thermogram. Several simplifying assumptions were made here. We assume instantaneous heating and cooling of the sample, and a uniform temperature profile along the 38 cm length of the TD oven. We also only consider gas-phase reactions, and neglect any surface-mediated reactions. When possible, JPL-recommended values for the rate constants were used, but many of those listed did not span the full temperature range of the thermograms. When JPL values were not available, reaction rates from the NIST database were used (see Table S1). We also derive temperature-dependent wall loss constants for O and OH using the procedure outlined by Thieser et al. (2016), but find that better agreement in some simulations can be achieved with the experimental data by using an empirical value, or no wall loss at all. As can be seen in Sect. 3, these simulations successfully replicated a major portion, but not all, of the experimental results, likely due to these simplifications.

3 Results

3.1 HNO_3 thermograms

Figure 2 shows the conversion efficiency of HNO_3 to NO_2 as a function of temperature, for several flow rates through the NOAA TD-CRDS. Conversion efficiency was calculated as the measured NO_2 mixing ratio divided by the input HNO_3 mixing ratio. The box model simulations for each flow rate are shown as solid lines of corresponding color. The HNO_3 permeation tube has a calibrated output of 64 ng/min, which corresponds to an expected HNO_3 concentration of between 5 and 40 ppbv, depending on the zero air dilution required for each flow rate. The output of the permeation tube was found to contain approximately 2.5% NO_2 and all HNO_3 thermograms have had this 2.5% baseline signal subtracted. At a flow rate of 1.9 slpm (where the oven residence time is 30 - 100 ms depending on temperature), we

observe 100% conversion of HNO_3 at oven temperatures above 600 °C, whereas the thermograms obtained at 1 slpm and 3 slpm reach a maximum conversion of 100% at 550 and 650 °C respectively. The 0.5 slpm thermogram has a slightly lower maximum conversion efficiency (95%), possibly due to the recombination reaction of OH and NO_2 during the extended time in the cool down region prior to detection.

The box model simulations in Fig. 2 mimic the shape of the experimental data, but some are slightly shifted to higher or lower temperatures, likely because the simulation is extremely sensitive to the flow rate and may be affected by the simplifying assumptions detailed in Sect. 2.4. The shape of the simulated thermogram is entirely controlled by the reaction rate of the initial dissociation reaction of HNO_3 to NO_2 + OH. This reaction has a third order rate constant of $k_0(T) = 1.82 \times 10^{-4} \cdot (T/298)^{-1.98} \cdot e^{(-24004/T)}$ and a high-pressure limit of $k_\infty(T) = 2 \times 10^{15} \cdot e^{(-24054/T)}$ (Glänzer and Troe, 1974) and thus at a midrange temperature such as 500 °C, the HNO_3 lifetime is approximately 250 ms. The inner volume of the oven is 4.5 cm^3, and so at a flow rate of 1.9 slpm, the gas has a plug flow residence time of 38 ms in the 500 °C oven, compared to a residence time of 77 ms at 1.0 slpm and 153 ms at 0.5 slpm. The simulated conversion efficiency in these mid-range temperatures is therefore extremely sensitive to the flow rate, in agreement with our experimental results. However, the experimental 100% conversion efficiency at high temperatures indicates that there is virtually no recombination of OH and NO_2 once formed, because the recombination rate for OH + NO_2 is quite low, and because OH radicals are far more likely to be lost to the walls of the oven at a diffusion-limited rate determined by Day et al. (2002) of ~46 s^{-1} for 1/4" OD tubing, which is far higher than the pseudo-first order recombination rate coefficient of 0.075 s^{-1} at $[NO_2]$ = 10 ppbv. No attempt was made to dilute the output of the HNO_3 permeation tube any further, as recombination effects would likely only be less important at lower starting HNO_3 concentrations. Similarly, increasing the starting NO_2 concentration, to mimic conditions in highly polluted environments, was not attempted in this set of experiments, but increasing the starting NO_2 concentration in the kinetic model up to 50 ppbv shows that there is no recombination expected even with elevated NO_2 in the oven. This is in contrast to ANs and PNs, for which the reaction of the dissociated peroxy and alkyl radicals with NO_2 is a significant interference (Thieser et al., 2016), but in good agreement with the HNO_3 results of Day et al. (2002) and Sobanski et al. (2016).

At a flow rate of 1.9 slpm, we observe a ~6% conversion of HNO_3 to NO_2 at an oven temperature of 400 °C. Although this efficiency is specific to the conditions of the oven used here, it is a key finding since 400 °C is in the vicinity of the temperature set point chosen for selective detection of total alkyl and multifunctional nitrates by TD-LIF (Day et al., 2002) and other TD instruments. This result is in good agreement with Thieser et al. (2016), who found a ~10% HNO_3 conversion at 450 °C. Sadanaga et al. (2016) report ~15% HNO_3 conversion at 360 °C at a TD residence time of 3.4 sec, which exceeds the

range of our study but follows the trend in Fig. 3. In a previous study (Wild et al., 2014), we presented thermograms designed to demonstrate quantitative conversion efficiency at high temperatures. The temperature dependence of thermal conversion was not well constrained at lower temperatures, and showed, for example, 30% conversion at 400 °C. As discussed by Sobanski et al. (2016), the large conversion efficiency presented by Wild et al. (2014) at this temperature is likely incorrect. The extent of HNO_3 conversion is dependent on the residence time in the oven, but because residence time for a given flow rate changes with oven temperature, it is easier to observe this effect by plotting conversion efficiency versus residence time, as in Fig. 3, for five different temperatures (350, 400, 450, 500, and 600 °C). This plot represents transects through Fig. 2 at these five temperatures. Figure S2 shows a log scale plot to highlight the low conversion efficiency region. Most instruments utilizing the TD oven technique use a set point between 350 and 450 degrees and a residence time between 30 and 100 ms to selectively detect ANs and not HNO_3 (Day et al., 2003;Paul et al., 2009;Thieser et al., 2016), but Fig. 3 demonstrates that there is significant variability in the HNO_3 conversion efficiency that depends nonlinearly on oven residence time.

We further measure the effect of pressure on the conversion by placing a heated stainless steel needle valve in front of the oven, thus lowering the pressure inside the oven to 250 mbar. The low pressure transects for each of the five temperatures can be seen in open circles in Fig. 3, and the full thermograms are displayed in Fig. S3. The low pressure transects are slightly lower than those at ambient pressure for the 450 and 500 °C setpoints, but match reasonably well at low and high temperatures, indicating that the onset and final conversion of HNO_3 are not strongly sensitive to pressure. To ensure that HNO_3 was not lost on the walls of the stainless steel valve, the conversion efficiency was measured with the valve fully open, and was found to match that taken with no valve. These experiments demonstrate the importance of verifying that a given temperature set point and flow rate is suitable for measurement of alkyl nitrates without interference from HNO_3 conversion.

To demonstrate the variability within individual TD ovens, an example of the HNO_3 conversion efficiency near the alkyl nitrate temperature setpoint, as measured by the Berkeley TD-LIF instrument, is shown in Fig. 4. This inlet's alkyl nitrate setpoint temperature was chosen to be just past the plateau in the n-propyl-nitrate signal at 410 °C. The HNO_3 conversion to NO_2 was found to be 2.5%, which for most TD-LIF experiments would be negligible compared to other uncertainties in measured ANs (±15%) and no correction would be applied. One example where a correction was significant was for the NASA DISCOVER-AQ California deployment, which took place in California's central valley during a period of high NH_4NO_3 aerosol loading. Ratios of (HNO_3 + NH_4NO_3) to ANs were high enough that a correction was necessary and applied to both observations (Pusede et al., 2016). As HNO_3 is derived by subtraction of the ANs, any HNO_3 conversion at the AN temperature results in a high bias for ANs and an equal low

bias for HNO_3. The sum of the two remains correct independent of the onset of the HNO_3 conversion. The Berkeley group has found the HNO_3 conversion to be oven dependent even for identical pressure and flow conditions indicating some but not all ovens have impurities at the walls that effectively catalyze HNO_3 decomposition. Ovens with high HNO_3 conversion efficiencies at low temperatures were discarded. These results highlight the importance of careful evaluation and calibration of each TD oven, even when the inner volumes and flow rates are similar.

3.2 HNO_3 thermograms with additions

Tests for other interferences to HNO_3 and AN measurements included adding several different chemical species to the HNO_3 sample prior to entering the oven. These were designed to test the hypothesis that certain trace gases found in ambient air would interact with radicals in the oven, or would themselves dissociate to form radicals which could react with NO, NO_2, OH, or HNO_3. The results are shown in Fig. 5. In Fig. 5a, a portion of the dilution air was passed through a distilled water bubbler prior to diluting the HNO_3, bringing the relative humidity up to 66%. The change in RH does not alter the shape, onset, or total conversion efficiency of the thermogram. This is to be expected, as the oven temperature is not high enough to dissociate H_2O to OH + H, and reactions between H_2O and the relevant species formed in the oven from HNO_3 dissociation are far too slow to be important here. However, it should be noted that both H_2O and HNO_3 are sampled in this experiment at a steady concentration, and it is possible that during ambient sampling, rapid changes in the RH or HNO_3 concentration could change the overall efficiency. Additionally, we did not test the conversion efficiency at very high RH levels, and it's possible there could be a non-linear effect of water. Figure 5b shows the measured thermogram with the addition of ~50 ppbv VOCs (described in Sect. 2.2) with and without the addition of 90 ppbv O_3, as well as the addition of 5 ppmv of propane, to mimic conditions found in highly polluted wintertime atmospheres If organic radicals were produced thermally in the TD oven, they could potentially react with NO_2, thus altering that signal. However, the bond dissociation energy of the C-H or C-C bonds most likely to thermally dissociate in each of the VOCs are all significantly higher (typically >100 kcal/mol) than that of the O-N bond in HNO_3 (~50 kcal/mol) making it unlikely that organic radicals are formed inside the oven from dissociation of VOCs. Reactions of unsaturated hydrocarbons with O atoms or OH radicals tend to be rapid and would produce organic radicals, but these tend to be unstable, and any stable radicals would likely only react with NO_2 to form ANs or PNs. The oven is set at sufficiently high temperatures to dissociate ANs and PNs back to NO_2 + the organic radical. Addition of these VOCs does not affect the measured conversion efficiency, even in the presence of ambient levels of O_3. Ozonolysis of the unsaturated hydrocarbons is slow enough (typically on the order of 1×10^{-17} cm^3 $molecule^{-1}$ s^{-1}) to not have any effect here (we would expect < 0.0001% reaction for the duration of the oven residence time).

An extremely high concentration of propane also has no effect on the overall conversion efficiency, within the error bars of the measurement, for the same reasons as detailed above.

Figure 5c shows the addition of both small and large quantities of O_3 to the HNO_3 sample. Small quantities do not change the onset or overall conversion efficiency, but larger amounts of O_3 reduce the conversion efficiency at high temperatures. The kinetic box model does not predict this reduction, as it predicts 100% conversion efficiency to NO_2 at all O_3 levels. The dominant bimolecular reaction of O_3 in the model is the reaction with NO_2 to make NO_3, but since these reactions are occurring at high temperature, any NO_3 formed will immediately dissociate to NO_2 (see Sect. 3.2). O_3 also thermally dissociates to $O + O_2$ at temperatures above 200 °C (see Fig. S4), but the dominant fate of the O radicals should be loss to the walls. Of the O atoms that are not lost to the walls, their primary reaction is also with NO_2 to form either $NO + O_2$ or NO_3 but NO should be converted back to NO_2 after the oven. Nevertheless, there is an apparent reduction in the conversion of HNO_3 to NO_2 with increasing O_3. While the O_3 concentration range in Fig. 5c exceeds that found in ambient air, highly polluted areas may have large enough O_3 concentrations to make this reduction in conversion efficiency significant. Finally, the addition of 400 ppmv CO in Fig. 5d has a marked effect on the onset, shape, and final conversion of the HNO_3. This addition was tested because gold catalytic NO_y converters require a 1% CO addition to drive the dissociation forward. We find that ~0.5% CO is sufficient to promote HNO_3 dissociation even in the absence of a gold catalyst. However, our kinetic model does not replicate the results of the CO addition. Since the rate-limiting step in these thermograms is the initial dissociation of HNO_3, it is unlikely that the reaction between CO and OH or NO_2 plays a role here. It must therefore be caused by a reaction which changes the rate kinetics of the initial dissociation step. However, to our knowledge there have been no laboratory kinetics studies on the $CO + HNO_3$ reaction. It is likely that there is some surface reaction that affects the HNO_3 conversion in the presence of CO.

We also note that previous work on TD ovens (Day et al., 2002;Thieser et al., 2016) has cautioned that the elevated temperature of the oven may accelerate the reaction between ambient levels of NO and O_3 to generate NO_2, thereby creating NO_2 signal that is in fact due to ambient levels of NO. This issue does not affect the TD-CRDS NO_y detection scheme, as excess O_3 is intentionally added to the mixing volume after the oven to convert NO to NO_2 to measure total NO_y. Nevertheless, we have investigated how NO responds in the oven, and the results are shown in Fig. S5. A 15 ppbv NO sample was passed through the oven. When no excess O_3 is added to the mixing volume, no NO_2 signal is seen, and when mixing volume O_3 is added, full conversion of NO to NO_2 is observed, as expected. However, when 100 ppbv of O_3 is added to the oven (with no mixing volume O_3 addition), approximately 2.2 ppbv NO_2 signal was observed, or a 15% conversion. This is consistent with the kinetic rate expressions for NO

+ O_3 and NO + O, but we do not differentiate between these two mechanisms in these experiments, as O_3 will always form O at the elevated oven temperatures.

3.2 N_2O_5 thermograms

Figure 6 shows the measured thermogram of N_2O_5 in the NOAA TD-CRDS at ambient pressure and flow rates of 1.9 and 1.0 slpm, with the kinetic model simulations for each flow rate shown in solid and dashed lines. Two distinct dissociation steps are observed and confirmed by the kinetic model, one between 30 and 110 °C corresponding to the dissociation of N_2O_5 to NO_2 + NO_3, and one above 300 °C corresponding to the dissociation of NO_3. The N_2O_5 synthesis method also produces HNO_3 (Bertram et al., 2009) and because the bond enthalpies of NO_3 and HNO_3 dissociation are similar (both ~50 kcal/mol), the thermograms of these two species are expected to overlap at high temperatures. Thus a nylon wool scrubber was used to remove HNO_3, and the scrubbed sample was simultaneously monitored with an iodide chemical ionization mass spectrometer, described in Sect. 2.3, to ensure the HNO_3 (and not the N_2O_5) was completely removed. The flow rate was lowered to 1.0 slpm in the high temperature scans to accommodate both instruments with better signal-to-noise. The CIMS measured approximately 120 pptv HNO_3, possibly due to hydrolysis of N_2O_5 after the scrubber, and thus more than 99.5% of the NO_2 signal we observe is attributed to N_2O_5.

At high temperatures, each N_2O_5 is expected to produce two NO_2 molecules. Conversion efficiency is calculated from the measured NO_2 concentration relative to the N_2O_5 concentration measured by the CIMS instrument, which samples prior to the TD oven. However, the CIMS instrument requires an empirical calibration factor for any species it measures, and while the HNO_3 signal may be calibrated using the permeation tube described in Sect. 3.1, there was no independent calibration available for N_2O_5 – only the signal measured using the TD-CRDS instrument. Therefore, the CIMS N_2O_5 signal was assumed to correspond to a 200% conversion efficiency in the TD-CRDS at 650 °C, and the relative conversion was measured at lower temperatures. The first dissociation step of N_2O_5 to NO_2 and NO_3 is expected at oven temperatures above 110 °C, but because the sample must then travel through a "cool down" region prior to entering the CRDS optical cavity (see Fig. 1), approximately 10% of the NO_2 and NO_3 is expected to recombine back to N_2O_5, based on the rate constant and the residence time in the mixing volume. This behavior has been well characterized previously (Fuchs et al., 2009) and is accounted for in the data analysis, and as expected, we observe a 91% conversion efficiency of N_2O_5 to NO_2 between 110 and 300 °C. At higher temperatures, NO_3 dissociates in the oven before recombining with NO_2, and thus a 200% conversion efficiency is observed. While this is not an absolute measure of conversion efficiency, the relative conversion efficiency is consistent with N_2O_5 dissociation and recombination reaction rates to generate two NO_2 molecules in a distinct stepwise manner. At 150 °C and

400 °C, the temperature setpoints often used for detection of PANs and ANs, we find 90% and 105% conversion of N_2O_5 to NO_2, respectively. The exact values are highly dependent on the residence time in both the oven and in the cool down region, but serve to highlight the importance of characterizing the N_2O_5 response in every thermal dissociation oven.

We also measured the conversion of N_2O_5 without the mixing volume O_3 addition at two relevant temperatures, in order to determine the mechanism for NO_3 dissociation. These data are shown in green triangles in Fig. 6, and show no difference in onset or maximum conversion efficiency whether or not mixing volume O_3 is added. As the mixing volume O_3 converts ambient or thermally produced NO to NO_2, the similarity of the two spectra indicates that the NO_3 dissociation mechanism must be $NO_3 \rightarrow NO_2 + O$. However, there are no published rate expressions for this reaction and the few studies on NO_3 thermal dissociation have disagreed about whether the reaction proceeds to $NO + O_2$ (Johnston et al., 1986) or $NO_2 + O$ (Schott and Davidson, 1958). The former argued for the $NO_3 \rightarrow NO + O_2$ mechanism based on thermodynamics, as this reaction is exothermic. However, this implies that NO_3 would be thermally unstable at room temperature, which is not the case. It is likely that there is a significant energy barrier to this reaction. The bond enthalpy of the $NO_3 \rightarrow NO_2 + O$ reaction, on the other hand, is 50.4 kcal/mol, nearly identical to that of $HNO_3 \rightarrow NO_2 + OH$, and the two thermograms are very similar in shape and are centered at the same temperature (500 °C). The simulation shown in Fig. 6 is a fit rate expression of $k(T) = 1 \times 10^{-2} \cdot (T/298)^{9} \cdot \exp(-1500/T)$ obtained by taking the rate expression of HNO_3 dissociation and iteratively adjusting it until it matched the data. Essentially identical results were observed in the TD-LIF instrument. (Cohen, 2016).

3.3 NH_4NO_3 thermograms

NH_4NO_3 particles were generated in situ from an aqueous solution, dried, and size-selected by a differential mobility analyzer (DMA) set at 250 nm prior to entering the TD oven. The conversion efficiency was calculated by comparing the measured NO_2 concentration in the TD-CRDS instrument to the expected number of NH_4NO_3 molecules in the aerosol particles, derived from the number and size of the aerosol particles as measured with an ultra-high sensitivity aerosol spectrometer (UHSAS). The measured UHSAS histogram was used, along with the literature value for the density of NH_4NO_3, to convert particle diameter to particle volume, and then to the total number of NH_4NO_3 molecules. We demonstrate here that the dissociation pathway is $NH_4NO_3 \rightarrow NH_3 + HNO_3$, and we assume that NH_3 is not converted in any significant fraction. A temperature-dependent baseline NO_2 signal is observed when the DMA voltage is set to zero (i.e. when no particles are transmitted) which is attributed to gas-phase HNO_3 molecules which have evaporated from the particles and adsorbed to the tubing walls, and which are subtracted from the total signal. Figure 7 shows the measured thermogram of NH_4NO_3 with the

thermogram of gas phase HNO_3 from Fig. 2 overlaid. The close agreement between the two thermograms demonstrates that the dissociation pathway is $NH_4NO_3 \rightarrow NH_3 + HNO_3$, and that this reaction is rapid at the temperatures reached in the TD inlet

For particles that pass through the DMA at a given size setpoint, the UHSAS measures a size histogram that peaks at a diameter approximately 8% lower, likely because the NH_4NO_3 particles are slightly non-spherical, and therefore the electrical mobility diameter is slightly larger than the geometric diameter. This phenomenon has been discussed at length elsewhere (DeCarlo et al., 2004), and we make no attempt to further characterize NH_4NO_3 particle behavior in the DMA – we have simply taken the UHSAS histogram data to calculate the particle volume, even though this is also subject to slight differences based on the refractive index of NH_4NO_3. However, if the TD oven failed to volatilize and convert all NH_4NO_3 particles to HNO_3 and then to NO_2, the measured thermogram would deviate from the HNO_3 spectrum at lower temperatures, where perhaps the heat is not sufficient to drive the NH_4NO_3 out of the condensed phase. The close match between the two is a good indication that the conversion goes to completion. Additionally, Figs. S6 and S7 show a sample NO_2 measurement measured by TD-CRDS at 650 °C as the particle diameter setpoint is changed. There is no correlation between particle size and conversion efficiency, indicating that the oven is completely converting all particles without a size dependence.

3.4 NH_3 thermograms

A previous study (Wild et al., 2014), investigated whether ambient levels of ammonia would represent an interference to NO_y conversion, and found that it made at most a 1% difference to the NO_2 signal in dry air, but that this effect was suppressed when RH > 10%. We find in the present study that there is a significant interference when ambient levels of both NH_3 and O_3 are present in the oven, but that this effect is potentially suppressed by other species found in ambient sampling. Figure 8 shows a thermogram of NH_3 with and without 100 ppbv O_3 present in the oven. The conversion of NH_3 to NO_2 at 650 °C, calculated as the observed NO_2 signal relative to the added NH_3 concentration, is small without O_3. This is consistent with the previous study of Wild et al. (2014). However, when 100 ppbv of O_3 is added, the thermogram reaches a maximum molar conversion efficiency of 8%, with an onset near 400 °C (red circles). In contrast to the HNO_3 thermograms, however, this signal does not appear to plateau at 650 °C but rather continues to grow at higher temperatures. This result is similar to the interference reported by Dillon et al. (2002), which was attributed to a reaction between NH_3 and O_3. The interference is only present when O_3 is added to the mixing volume, indicating that the conversion of NH_3 must be producing NO, rather than NO_2, and is subsequently unimportant to instruments that measure NO_2 only, such as TD-LIF instruments. A kinetic model simulation of both experiments is shown in solid line in Fig. 8. This

simulation was carried out with 35 relevant reactions between NH_3, O_3, and the radicals that are formed from these two species in the oven, with the most important reactions are listed below. The reaction between NH_3 and O_3 is far too slow to be relevant here, and the oven temperature is not high enough to dissociate NH_3 to NH_2 + H (ΔH = 108 kcal/mol). However, O_3 dissociates readily at oven temperatures above 200 °C, and once formed, the O atoms may react with NH_3 to form NH_2.

$$O_3 \rightarrow O_2 + O \quad (3)$$

$$NH_3 + O \rightarrow NH_2 + OH$$

$$NH_3 + OH \rightarrow NH_2 + H_2O$$

The reactions of NH_3 are the slowest steps, but once formed, NH_2 reacts readily with O atoms.

$$NH_2 + O \rightarrow HNO + H \quad (4)$$
$$\rightarrow OH + NH$$
$$\rightarrow NO + H_2$$

HNO then reacts with O, OH, and H to form NO, or can also directly dissociate to form H + NO.

$$HNO + O \rightarrow OH + NO \quad (5)$$

$$HNO + OH \rightarrow H_2O + NO$$

$$HNO + H \rightarrow H_2 + NO$$

$$HNO \rightarrow H + NO$$

The OH and H atoms formed in Eq. (4) and (5) then drive Eq. (3) further. This mechanism takes place entirely in the gas phase, and does not take into account any surface-mediated reactions. Many of these reactions have only limited published studies, so the simulation used rate constants that have not been extensively tested. Additionally, to achieve a significant conversion of NH_3 to NO, it was necessary to decrease the O and OH wall loss constants in the model. This rudimentary simulation predicts the initial signal increase starting at 300 °C, though it has a maximum conversion efficiency of just under 2%, which is below that observed in the experiment. In Fig. 9, we adjusted the amount of added O_3, while monitoring the conversion efficiency of NH_3 to NO_2 at an inlet temperature of 650 °C. We find that increasing the O_3 increases the conversion, which is consistent with NH_3 + O being the limiting reaction to make NH_2. Figure 9 also demonstrates that the conversion of NH_3 is partially quenched by the addition of ambient levels (~100 ppbv) of CO, likely because the CO + O $\rightarrow$ CO_2 reaction competes with those in Eq. (3). Figure 10 shows that the average conversion efficiency of NH_3 when measured in ambient air in Boulder, CO in August 2016 (which contains 40-60 ppbv O_3, >80 ppbv CO, ~15% RH, and other species) is 0.5 ± 2.4%, or zero to within the 1σ error from repeated measurements. This is in contrast to the conversion efficiency of HNO_3 in ambient air, shown in the upper right frame of Fig. 10, which is largely unchanged from that measured in zero air. Thus, constituents present in ambient air, such as methane,

CO, and water, are possibly suppressing the conversion of NH_3 to NO, likely through the reaction with O atoms.

4 Discussion

Using a thermal-dissociation cavity ringdown spectrometer (TD-CRDS), we have quantitatively added reactive nitrogen species to the TD inlet, in order to test the efficiency of the thermal conversion of each species to NO_2, and the effect of any interferences from other trace gases which may be present in the ambient troposphere. We have determined that the TD-CRDS converts HNO_3, N_2O_5, and NH_4NO_3 particles to NO_2 with 100% efficiency at temperatures above 600 °C, but that the onsets of the dissociation are highly dependent on oven residence time. Despite their similar residence times, the NOAA TD-CRDS and Berkeley TD-LIF instruments measure HNO_3 conversion efficiencies ranging from 2.5% to ~8% at 410 °C. It is therefore important that the oven residence time is well characterized in instruments designed to selectively detect ANs without interference from HNO_3. Even two TD ovens with identical inner volumes may exhibit different response functions if they have different ratios of surface area to volume.

We find that high levels of ambient O_3 (>500 ppbv) and CO (>400 ppmv) significantly changed the final conversion efficiency and the onset of the conversion, respectively, of the HNO_3 thermogram, but that ambient levels of a group of representative VOCs and high RH did not affect the measured thermogram. Modest levels of O_3 converted a portion of NH_3 to NO_2. The conversion mechanism likely arises from a gas-phase reaction between oxygen atoms and NH_3 which produces NO. To our knowledge, the $NH_3 + O_3$ reaction in TD ovens has not been studied in detail, but previous studies of NH_3 conversion in catalytic converters have noted similar results to those presented here – water and CO suppress the NH_3 conversion to NO, while O_3 enhances it (Fahey et al., 1985;Kliner et al., 1997). If not quenched by other species present in ambient air, this effect could represent a potentially significant interference in field sampling for instruments that are sensitive to NO directly, or via conversion to NO_2. For example, at 50 ppbv O_3, the 6% conversion of NH_3 would present an interference of more than 10% if $NH_3/NO_y > 1.7$, which is not an uncommon condition in agricultural regions. This signal was suppressed in ambient air, indicating that NH_3 may not interfere with NO_y under most conditions. However, ambient air in Boulder is not representative of all sampling conditions, and since the species responsible for quenching the reaction remains unclear, more work must be done to better understand the mechanism of the NH_3/O_3 thermal reaction. This result, along with the others detailed above, serve to emphasize that great care must be taken to characterize the potential interferences in TD NO_y-conversion ovens.

The measured N_2O_5 thermogram exhibits a double dissociation curve, corresponding to the initial dissociation of N_2O_5 to NO_2 and NO_3, and the subsequent dissociation of NO_3. Our results indicate that the mechanism of the second step is $NO_3 \rightarrow NO_2 + O$, in contrast to earlier literature that reported $NO_3 \rightarrow NO + O_2$ as the dominant mechanism. To our knowledge, this is the first published thermogram of NO_3. TD-NO_y instruments often operate in the daytime when N_2O_5 is not a significant fraction of NO_y, though some groups have operated at night and have typically assumed complete conversion to $NO_2 + NO_3$ at the TD inlet setpoint for PNs (Di Carlo et al., 2013), and complete conversion to $2NO_2 + O$ at the setpoint for HNO_3 (Wild et al., 2014). These results confirm that there is approximately quantitative conversion at these setpoints, though there are slight deviations from 100% conversion near the PN setpoint. Therefore, care must be taken to select a setpoint carefully and ensure complete conversion at that temperature. However, this interference would only be significant during nighttime or during very cold weather sampling.

The thermogram of particulate ammonium nitrate matches the thermogram of HNO_3, within the margin of error of the UHSAS measurement. TD ovens have not typically been used explicitly for particle detection, with a few exceptions (Voisin et al., 2003;Smith et al., 2004;Rollins et al., 2010), though very fine particles may be sampled by the inlet, unless they are excluded aerodynamically or physically. These results demonstrate that the volatile portion of the particulate ammonium nitrates will be driven into the gas phase at low oven temperatures, consistent with Rollins et al. (2010), who used a denuder to remove gas phase nitrates and to detect aerosol organic nitrates in a 325 °C oven. Their results indicate it is likely that particulate organic nitrates would be converted to NO_2 with 100% efficiency in the NOAA TD-CRDS, but this result has not been explicitly tested here. Other NO_3 salts might also be detected via thermal dissociation, although it is expected that they would be non-volatile at the temperatures of these TD-inlets. Bertram and Cohen (2003) examined $NaNO_3$ and determined that those particles would not be detected in TD inlets. However, these studies measured pure aerosols, and results may vary with heterogeneously mixed particles with multiple components. The initial dissociation of NH_4NO_3 will produce an NH_3 molecule in addition to an HNO_3 molecule, which means that particles may be subject to the same NH_3/O_3 interference when sampling in ambient air, which was not considered in this study. Additionally, the particles sampled in this paper were generated and injected directly into the inlet. The efficiency of particle sampling in ambient air will depend on particle size and inlet design, particularly during aircraft measurements. In future studies, a TD inlet that either effectively samples aerosol, or effectively excludes aerosol (such as a cyclone), or a combination of the two could be used to specifically measure aerosol nitrates, which may make up a substantial fraction of NO_y, particularly in polluted wintertime urban atmospheres.

Based on the results of this paper, we make the following three recommendations: *(1)* TD ovens should be characterized with the appropriate reactive nitrogen compounds regularly at the oven set points using the oven residence time and gas pressure that will be used in ambient sampling. This is especially important given the findings of the Berkeley group regarding impurities found in otherwise identical ovens, as discussed in Sect. 3.1. *(2)* In addition to the AN and PN calibrations recommended by (Day et al., 2002;Thieser et al., 2016) and others, these calibrations should include HNO_3. HNO_3 calibration will be especially important if sampling in regions where HNO_3 is in large excess over other NO_y species. *(3)* Potential non-NO_y species such as NH_3 should also be regularly introduced into the inlet under conditions where O_3 is present in ambient air to check for potential conversion. These recommendations are similar to those detailed in Bradshaw et al. (1998). The results of Fig. 9 indicate that calibration results may also vary significantly when sampling in ambient air, due to the large number of possible gas-phase reactions available to the wide variety of trace atmospheric species. The last step is particularly important in instruments that detect NO as well as NO_2. Comprehensive calibration of these instruments NO_y measurement accuracy, which in turn will provide valuable information about tropospheric NO_x chemistry.

Acknowledgements

We would like to thank Douglas Day for his advice on the construction and deployment of TD inlets, and Jim Roberts, Tom Ryerson, Dave Parrish, and Joel Thornton for other helpful discussions. We also wish to thank Jessica Gilman for providing the GC/MS VOC mixture, Sascha Albrecht for measuring the NO_2 baseline in the HNO_3 permeation tube, and Jim Burkholder for the loan of a propane tank. CCW acknowledges support from the National Research Council Research Associateship Program. The authors acknowledge support from the Atmospheric Chemistry, Carbon Cycle and Climate Program (AC4).

References

Beaver, M. R., Clair, J. M. S., Paulot, F., Spencer, K. M., Crounse, J. D., LaFranchi, B. W., Min, K. E., Pusede, S. E., Wooldridge, P. J., Schade, G. W., Park, C., Cohen, R. C., and Wennberg, P. O.: Importance of biogenic precursors to the budget of organic nitrates: observations of multifunctional organic nitrates by CIMS and TD-LIF during BEARPEX 2009, Atmos. Chem. Phys., 12, 5773-5785, 10.5194/acp-12-5773-2012, 2012.

Bertram, T. H., and Cohen, R. C.: A prototype instrument for the real time detection of semi-volatile organic and inorganic nitrate aerosol, Eos Trans. AGU, 84(46), Fall Meet. Suppl., Abstract A51F-0740, 2003,

Bertram, T. H., Thornton, J. A., and Riedel, T. P.: An experimental technique for the direct measurement of N_2O_5 reactivity on ambient particles, Atmos. Meas. Tech., 2, 231-242, 10.5194/amt-2-231-2009, 2009.

Bradshaw, J., Sandholm, S., and Talbot, R.: An update on reactive odd-nitrogen measurements made during recent NASA Global Tropospheric Experiment programs, J. Geophys. Res - Atmos, 103, 19129-19148, 10.1029/98JD00621, 1998.

Cai, Y., Montague, D. C., Mooiweer-Bryan, W., and Deshler, T.: Performance characteristics of the ultra high sensitivity aerosol spectrometer for particles between 55 and 800 nm: Laboratory and field studies, J. Aerosol Sci., 39, 759-769, 10.1016/j.jaerosci.2008.04.007, 2008.

Cohen, R. C.: Private communication, WINTER data workshop, 2016.

Crosley, D. R.: NO_y Blue Ribbon panel, J. Geophys. Res - Atmos, 101, 2049-2052, 10.1029/95JD02276, 1996.

Darley, E. F., Kettner, K. A., and Stephens, E. R.: Analysis of peroxyacyl nitrates by gas chromatography with electron capture detection, Anal. Chem., 35, 589-591, 10.1021/ac60197a028, 1963.

Davidson, J. A., Viggiano, A. A., Howard, C. J., Dotan, I., Fehsenfeld, F. C., Albritton, D. L., and Ferguson, E. E.: Rate constants for the reactions of O_2^+, NO_2^+, NO^+, H_3O^+, CO_3^-, NO_2^-, and halide ions with N_2O_5 at 300 K, J. Chem. Phys., 68, 2085-2087, 10.1063/1.436032, 1978.

Day, D. A., Wooldridge, P. J., Dillon, M. B., Thornton, J. A., and Cohen, R. C.: A thermal dissociation laser-induced fluorescence instrument for in situ detection of NO_2, peroxy nitrates, alkyl nitrates, and HNO_3, J. Geophys. Res., 107, 10.1029/2001jd000779, 2002.

Day, D. A., Dillon, M. B., Wooldridge, P. J., Thornton, J. A., Rosen, R. S., Wood, E. C., and Cohen, R. C.: On alkyl nitrates, O_3, and the "missing NO_y", J. Geophys. Res., 108, 10.1029/2003jd003685, 2003.

DeCarlo, P. F., Slowik, J. G., Worsnop, D. R., Davidovits, P., and Jimenez, J. L.: Particle morphology and density characterization by combined mobility and aerodynamic diameter measurements. Part 1: Theory, Aerosol Sci. Tech., 38, 1185-1205, 10.1080/027868290903907, 2004.

Di Carlo, P., Aruffo, E., Busilacchio, M., Giammaria, F., Dari-Salisburgo, C., Biancofiore, F., Visconti, G., Lee, J., Moller, S., Reeves, C. E., Bauguitte, S., Forster, G., Jones, R. L., and Ouyang, B.: Aircraft based four-channel thermal dissociation laser induced fluorescence instrument for simultaneous measurements of NO₂, total peroxy nitrate, total alkyl nitrate, and HNO₃, Atmos. Meas. Tech., 6, 971-980, 10.5194/amt-6-971-2013, 2013.

Dillon, M. B., Lamanna, M. S., Schade, G. W., Goldstein, A. H., and Cohen, R. C.: Chemical evolution of the Sacramento urban plume: Transport and oxidation, J. Geophys. Res - Atmos, 107, ACH 3-1-ACH 3-15, 10.1029/2001JD000969, 2002.

Dubé, W. P., Brown, S. S., Osthoff, H. D., Nunley, M. R., Ciciora, S. J., Paris, M. W., McLaughlin, R. J., and Ravishankara, A. R.: Aircraft instrument for simultaneous, in situ measurement of NO_3 and N_2O_5 via pulsed cavity ring-down spectroscopy, Rev. Sci. Instrum., 77, 034101, 10.1063/1.2176058, 2006.

EPA: 8-Hour ozone nonattainment areas (2008 standard) in EPA Green Book, available at: http://www.epa.gov/airquality/greenbook/map8hr_2008.html, 2016.

Fahey, D. W., Eubank, C. S., Hübler, G., and Fehsenfeld, F. C.: Evaluation of a catalytic reduction technique for the measurement of total reactive odd-nitrogen NO_y in the atmosphere, J. Atmos. Chem., 3, 435-468, 10.1007/bf00053871, 1985.

Fahey, D. W., Hübler, G., Parrish, D. D., Williams, E. J., Norton, R. B., Ridley, B. A., Singh, H. B., Liu, S. C., and Fehsenfeld, F. C.: Reactive nitrogen species in the troposphere: Measurements of NO, NO_2,HNO_3, particulate nitrate, peroxyacetyl nitrate (PAN), O_3, and total reactive odd nitrogen (NO_y) at Niwot Ridge, Colorado, J. Geophys. Res., 91, 9781-9793, 1986.

Fehsenfeld, F. C., Huey, L. G., Sueper, D. T., Norton, R. B., Williams, E. J., Eisele, F. L., Mauldin, R. L., and Tanner, D. J.: Ground-based intercomparison of nitric acid measurement techniques, J. Geophys. Res - Atmos, 103, 3343-3353, 10.1029/97JD02213, 1998.

Flocke, F. M., Weinheimer, A. J., Swanson, A. L., Roberts, J. M., Schmitt, R., and Shertz, S.: On the measurement of PANs by gas chromatography and electron capture detection, J. Atmos. Chem., 52, 19-43, 10.1007/s10874-005-6772-0, 2005.

Fuchs, H., Dubé, W. P., Lerner, B. M., Wagner, N. L., Williams, E. J., and Brown, S. S.: A sensitive and versatile detector for atmospheric NO_2 and NO_x based on blue diode laser cavity ring-down spectroscopy, Environ. Sci. Technol., 43, 7831-7836, 10.1021/es902067h, 2009.

Glänzer, K., and Troe, J.: Thermal decomposition of nitrocompounds in shock waves. IV: Decomposition of nitric acid, Berich. Bunsen. Gesell., 78, 71-76, 10.1002/bbpc.19740780112, 1974.

Huey, L. G., Dunlea, E. J., Lovejoy, E. R., Hanson, D. R., Norton, R. B., Fehsenfeld, F. C., and Howard, C. J.: Fast time response measurements of HNO_3 in air with a chemical ionization mass spectrometer, J. Geophys. Res - Atmos, 103, 3355-3360, 10.1029/97JD02214, 1998.

Huey, L. G.: Measurement of trace atmospheric species by chemical ionization mass spectrometry: Speciation of reactive nitrogen and future directions, Mass Spectrom. Rev., 26, 166-184, 10.1002/mas.20118, 2007.

Johnston, H. S., Cantrell, C. A., and Calvert, J. G.: Unimolecular decomposition of NO_3 to form NO and O_2 and a review of N_2O_5/NO_3 kinetics, J. Geophys. Res - Atmos, 91, 5159-5172, 10.1029/JD091iD04p05159, 1986.

Kercher, J. P., Riedel, T. P., and Thornton, J. A.: Chlorine activation by N_2O_5: simultaneous, in situ detection of $ClNO_2$ and N_2O_5 by chemical ionization mass spectrometry, Atmos. Meas. Tech., 2, 193-204, 10.5194/amt-2-193-2009, 2009.

King, M. D., Dick, E. M., and Simpson, W. R.: A new method for the atmospheric detection of the nitrate radical (NO₃), Atmos. Environ., 34, 685-688, http://dx.doi.org/10.1016/S1352-2310(99)00418-5, 2000.

Kley, D., and McFarland, M.: Chemiluminescence detector for NO and NO_2, Atmospheric Technology, 12, 63-69, 1980.

Kliner, D. A. V., Daube, B. C., Burley, J. D., and Wofsy, S. C.: Laboratory investigation of the catalytic reduction technique for measurement of atmospheric NO_y, J. Geophys. Res - Atmos, 102, 10759-10776, 10.1029/96JD03816, 1997.

Lee, B. H., Lopez-Hilfiker, F. D., Mohr, C., Kurtén, T., Worsnop, D. R., and Thornton, J. A.: An iodide-adduct high-resolution time-of-flight chemical-ionization mass spectrometer: Application to atmospheric inorganic and organic compounds, Environ. Sci. Technol., 48, 6309-6317, 10.1021/es500362a, 2014.

Lee, B. H., Mohr, C., Lopez-Hilfiker, F. D., Lutz, A., Hallquist, M., Lee, L., Romer, P., Cohen, R. C., Iyer, S., Kurtén, T., Hu, W., Day, D. A., Campuzano-Jost, P., Jimenez, J. L., Xu, L., Ng, N. L., Guo, H., Weber, R. J., Wild, R. J., Brown, S. S., Koss, A., de Gouw, J., Olson, K., Goldstein, A. H., Seco, R., Kim, S., McAvey, K., Shepson, P. B., Starn, T., Baumann, K., Edgerton, E. S., Liu, J., Shilling, J. E., Miller, D. O., Brune, W., Schobesberger, S., D'Ambro, E. L., and Thornton, J. A.: Highly functionalized organic nitrates in the southeast United States: Contribution to secondary organic aerosol and reactive nitrogen budgets, Proc. Natl. Acad. Sci. USA, 113, 1516-1521, 10.1073/pnas.1508108113, 2016.

Manion, J. A., Huie, R. E., Levin, R. D., Jr., D. R. B., Orkin, V. L., Tsang, W., McGivern, W. S., Hudgens, J. W., Knyazev, V. D., Atkinson, D. B., Chai, E., Tereza, A. M., Lin, C.-Y., Allison, T. C., Mallard, W. G., Westley, F., Herron, J. T., Hampson, R. F., and Frizzell, D. H.: NIST Chemical Kinetics Database, NIST Standard Reference Database 17, Version 7.0 (Web Version), Release 1.6.8, Data version 2015.12, 2015.

Neuman, J. A., Huey, L. G., Ryerson, T. B., and Fahey, D. W.: Study of inlet materials for sampling atmospheric nitric acid, Environ. Sci. Technol., 33, 1133-1136, 10.1021/es980767f, 1999.

Neuman, J. A., Huey, L. G., Dissly, R. W., Fehsenfeld, F. C., Flocke, F., Holecek, J. C., Holloway, J. S., Hübler, G., Jakoubek, R., Nicks, D. K., Parrish, D. D., Ryerson, T. B., Sueper, D. T., and Weinheimer, A. J.: Fast-response airborne in situ measurements of HNO_3 during the Texas 2000 Air Quality Study, J. Geophys. Res - Atmos, 107, 4436, 10.1029/2001JD001437, 2002.

Neuman, J. A., Ryerson, T. B., Huey, L. G., Jakoubek, R., Nowak, J. B., Simons, C., and Fehsenfeld, F. C.: Calibration and evaluation of nitric acid and ammonia permeation tubes by UV optical absorption, Environ. Sci. Technol., 37, 2975, 10.1021/es026422l, 2003.

Neuman, J. A., Aikin, K. C., Atlas, E. L., Blake, D. R., Holloway, J. S., Meinardi, S., Nowak, J. B., Parrish, D. D., Peischl, J., Perring, A. E., Pollack, I. B., Roberts, J. M., Ryerson, T. B., and Trainer, M.: Ozone and alkyl nitrate formation from the Deepwater Horizon oil spill atmospheric emissions, J. Geophys. Res - Atmos, 117, D09305, 10.1029/2011JD017150, 2012.

Nikitas, C., Clemitshaw, K. C., Oram, D. E., and Penkett, S. A.: Measurement of PAN in the polluted boundary layer and free troposphere using a luminol-NO_2 detector combined with a thermal converter, J. Atmos. Chem., 28, 339-359, 10.1023/A:1005898017520, 1997.

O'Brien, J. M., Shepson, P. B., Muthuramu, K., Hao, C., Niki, H., Hastie, D. R., Taylor, R., and Roussel, P. B.: Measurements of alkyl and multifunctional organic nitrates at a rural site in Ontario, J. Geophys. Res - Atmos, 100, 22795-22804, 10.1029/94JD03247, 1995.

O'Keefe, A., and Deacon, D. A. G.: Cavity ring-down optical spectrometer for absorption measurements using pulsed laser sources, Rev. Sci. Instrum., 59, 2544-2551, 10.1063/1.1139895, 1988.

Paul, D., Furgeson, A., and Osthoff, H. D.: Measurements of total peroxy and alkyl nitrate abundances in laboratory-generated gas samples by thermal dissociation cavity ring-down spectroscopy, Rev. Sci. Instrum., 80, 114101, 10.1063/1.3258204, 2009.

Pérez, I. M., Wooldridge, P. J., and Cohen, R. C.: Laboratory evaluation of a novel thermal dissociation chemiluminescence method for in situ detection of nitrous acid, Atmos. Environ., 41, 3993-4001, http://dx.doi.org/10.1016/j.atmosenv.2007.01.060, 2007.

Perner, D., and Platt, U.: Detection of nitrous acid in the atmosphere by differential optical absorption, Geophysical Research Letters, 6, 917-920, 10.1029/GL006i012p00917, 1979.

Phillips, G. J., Pouvesle, N., Thieser, J., Schuster, G., Axinte, R., Fischer, H., Williams, J., Lelieveld, J., and Crowley, J. N.: Peroxyacetyl nitrate (PAN) and peroxyacetic acid (PAA) measurements by iodide chemical ionisation mass spectrometry: first analysis of results in the boreal forest and implications for the measurement of PAN fluxes, Atmos. Chem. Phys., 13, 1129-1139, 10.5194/acp-13-1129-2013, 2013.

Pusede, S. E., Duffey, K. C., Shusterman, A. A., Saleh, A., Laughner, J. L., Wooldridge, P. J., Zhang, Q., Parworth, C. L., Kim, H., Capps, S. L., Valin, L. C., Cappa, C. D., Fried, A., Walega, J., Nowak, J. B., Weinheimer, A. J., Hoff, R. M., Berkoff, T. A., Beyersdorf, A. J., Olson, J., Crawford, J. H., and Cohen, R. C.: On the effectiveness of nitrogen oxide reductions as a control over ammonium nitrate aerosol, Atmos. Chem. Phys., 16, 2575-2596, 10.5194/acp-16-2575-2016, 2016.

Ridley, B. A., and Howlett, L. C.: An instrument for nitric oxide measurements in the stratosphere, Rev. Sci. Instrum., 45, 742-746, doi:http://dx.doi.org/10.1063/1.1686726, 1974.

Rollins, A. W., Smith, J. D., Wilson, K. R., and Cohen, R. C.: Real time in situ detection of organic nitrates in atmospheric aerosols, Environ. Sci. Technol., 44, 5540-5545, 10.1021/es100926x, 2010.

Sadanaga, Y., Takaji, R., Ishiyama, A., Nakajima, K., Matsuki, A., and Bandow, H.: Thermal dissociation cavity attenuated phase shift spectroscopy for continuous measurement of total peroxy and organic nitrates in the clean atmosphere, Rev. Sci. Instrum., 87, 074102, doi:http://dx.doi.org/10.1063/1.4958167, 2016.

Sander, S. P., Abbatt, J., Barker, J. R., Burkholder, J. B., Friedl, R. R., Golden, D. M., Huie, R. E., Kolb, C. E., Kurylo, M. J., Moortgat, G. K., Orkin, V. L., and Wine, P. H.: Chemical kinetics and photochemical data for use in atmospheric studies. Evaluation No. 17 (http://jpldataeval.jpl.nasa.gov/), 2011.

Schott, G., and Davidson, N.: Shock waves in chemical kinetics: The decomposition of N_2O_5 at high temperatures, J. Am. Chem. Soc., 80, 1841-1853, 10.1021/ja01541a019, 1958.

Slusher, D. L., Huey, L. G., Tanner, D. J., Flocke, F. M., and Roberts, J. M.: A thermal dissociation–chemical ionization mass spectrometry (TD-CIMS) technique for the simultaneous measurement of peroxyacyl nitrates and dinitrogen pentoxide, J. Geophys. Res - Atmos, 109, D19315, 10.1029/2004JD004670, 2004.

Smith, J. N., Moore, K. F., McMurry, P. H., and Eisele, F. L.: Atmospheric measurements of sub-20 nm diameter particle chemical composition by thermal desorption chemical ionization mass spectrometry, Aerosol Sci. Tech., 38, 100-110, 10.1080/02786820490249036, 2004.

Sobanski, N., Schuladen, J., Schuster, G., Lelieveld, J., and Crowley, J.: A 5-channel cavity ring-down spectrometer for the detection of NO_2, NO_3, N_2O_5, total peroxy nitrates and total alkyl nitrates, Atmos. Meas. Tech. Discuss., 2016, 1-32, 10.5194/amt-2016-191, 2016.

Talbot, R. W., Vijgen, A. S., and Harriss, R. C.: Measuring tropospheric HNO_3: Problems and prospects for nylon filter and mist chamber techniques, J. Geophys. Res - Atmos, 95, 7553-7561, 10.1029/JD095iD06p07553, 1990.

Thaler, R. D., Mielke, L. H., and Osthoff, H. D.: Quantification of nitryl chloride at part per trillion mixing ratios by thermal dissociation cavity ring-down spectroscopy, Anal. Chem., 83, 2761-2766, 10.1021/ac200055z, 2011.

Thieser, J., Schuster, G., Schuladen, J., Phillips, G. J., Reiffs, A., Parchatka, U., Pöhler, D., Lelieveld, J., and Crowley, J. N.: A two-channel thermal dissociation cavity ring-down spectrometer for the detection of ambient NO_2, RO_2NO_2 and $RONO_2$, Atmos. Meas. Tech., 9, 553-576, 10.5194/amt-9-553-2016, 2016.

Thornton, J. A., Wooldridge, P. J., and Cohen, R. C.: Atmospheric NO_2: In situ laser-induced fluorescence detection at parts per trillion mixing ratios, Anal. Chem., 72, 528-539, 10.1021/ac9908905, 2000.

Veres, P. R., Roberts, J. M., Wild, R. J., Edwards, P. M., Brown, S. S., Bates, T. S., Quinn, P. K., Johnson, J. E., Zamora, R. J., and de Gouw, J.: Peroxynitric acid (HO_2NO_2) measurements during the UBWOS 2013 and 2014 studies using iodide ion chemical ionization mass spectrometry, Atmos. Chem. Phys., 15, 8101-8114, 10.5194/acp-15-8101-2015, 2015.

Voisin, D., Smith, J. N., Sakurai, H., McMurry, P. H., and Eisele, F. L.: Thermal desorption chemical ionization mass spectrometer for ultrafine particle chemical composition, Aerosol Sci. Tech., 37, 471-475, 10.1080/02786820300959, 2003.

Wagner, N. L., Dubé, W. P., Washenfelder, R. A., Young, C. J., Pollack, I. B., Ryerson, T. B., and Brown, S. S.: Diode laser-based cavity ring-down instrument for NO_3, N_2O_5, NO, NO_2 and O_3 from aircraft, Atmos. Meas. Tech., 4, 1227-1240, 10.5194/amt-4-1227-2011, 2011.

Washenfelder, R. A., Wagner, N. L., Dubé, W. P., and Brown, S. S.: Measurement of atmospheric ozone by cavity ring-down spectroscopy, Environ. Sci. Technol., 45, 2938-2944, 10.1021/es103340u, 2011.

Wild, R. J., Edwards, P. M., Dubé, W. P., Baumann, K., Edgerton, E. S., Quinn, P. K., Roberts, J. M., Rollins, A. W., Veres, P. R., Warneke, C., Williams, E. J., Yuan, B., and Brown, S. S.: A measurement of total reactive nitrogen, NO_y, together with NO_2, NO, and O_3 via cavity ring-down spectroscopy, Environ. Sci. Technol., 48, 9609-9615, 10.1021/es501896w, 2014.

Wild, R. J., Edwards, P. M., Bates, T. S., Cohen, R. C., de Gouw, J. A., Dubé, W. P., Gilman, J. B., Holloway, J., Kercher, J., Koss, A. R., Lee, L., Lerner, B. M., McLaren, R., Quinn, P. K., Roberts, J. M., Stutz, J., Thornton, J. A., Veres, P. R., Warneke, C., Williams, E., Young, C. J., Yuan, B., Zarzana, K. J., and Brown, S. S.: Reactive nitrogen partitioning and its relationship to winter ozone events in Utah, Atmos. Chem. Phys., 16, 573-583, 10.5194/acp-16-573-2016, 2016.

Williams, E. J., Baumann, K., Roberts, J. M., Bertman, S. B., Norton, R. B., Fehsenfeld, F. C., Springston, S. R., Nunnermacker, L. J., Newman, L., Olszyna, K., Meagher, J., Hartsell, B., Edgerton, E., Pearson, J. R., and Rodgers, M. O.: Intercomparison of ground-based NO_y measurement techniques, J. Geophys. Res - Atmos, 103, 22261-22280, 10.1029/98JD00074, 1998.

Winer, A. M., Peters, J. W., Smith, J. P., and Pitts, J. N.: Response of commercial chemiluminescent nitric oxide-nitrogen dioxide analyzers to other nitrogen-containing compounds, Environ. Sci. Technol., 8, 1118-1121, 10.1021/es60098a004, 1974.

Wooldridge, P. J., Perring, A. E., Bertram, T. H., Flocke, F. M., Roberts, J. M., Singh, H. B., Huey, L. G., Thornton, J. A., Wolfe, G. M., Murphy, J. G., Fry, J. L., Rollins, A. W., LaFranchi, B. W., and Cohen, R. C.: Total peroxy nitrates (ΣPNs) in the atmosphere: the Thermal Dissociation-Laser Induced Fluorescence (TD-LIF) technique and comparisons to speciated PAN measurements, Atmos. Meas. Tech., 3, 593-607, 10.5194/amt-3-593-2010, 2010.

Worton, D. R., Mills, G. P., Oram, D. E., and Sturges, W. T.: Gas chromatography negative ion chemical ionization mass spectrometry: Application to the detection of alkyl nitrates and halocarbons in the atmosphere, J. Chromatogr. A, 1201, 112-119, http://dx.doi.org/10.1016/j.chroma.2008.06.019, 2008.

Xiong, F., McAvey, K. M., Pratt, K. A., Groff, C. J., Hostetler, M. A., Lipton, M. A., Starn, T. K., Seeley, J. V., Bertman, S. B., Teng, A. P., Crounse, J. D., Nguyen, T. B., Wennberg, P. O., Misztal, P. K., Goldstein, A. H., Guenther, A. B., Koss, A. R., Olson, K. F., de Gouw, J. A., Baumann, K., Edgerton, E.

S., Feiner, P. A., Zhang, L., Miller, D. O., Brune, W. H., and Shepson, P. B.: Observation of isoprene hydroxynitrates in the southeastern United States and implications for the fate of NO_x, Atmos. Chem. Phys., 15, 11257-11272, 10.5194/acp-15-11257-2015, 2015.

Zheng, W., Flocke, F. M., Tyndall, G. S., Swanson, A., Orlando, J. J., Roberts, J. M., Huey, L. G., and Tanner, D. J.: Characterization of a thermal decomposition chemical ionization mass spectrometer for the measurement of peroxy acyl nitrates (PANs) in the atmosphere, Atmos. Chem. Phys., 11, 6529-6547, 10.5194/acp-11-6529-2011, 2011.

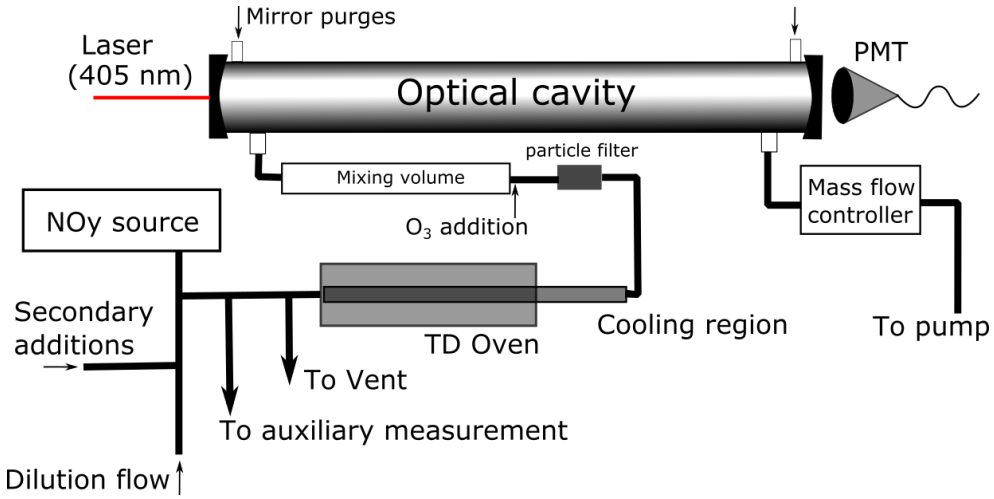

Figure 1: Instrument schematic of the TD-CRDS instrument used in this study. An NO_y source (HNO_3 permeation tube, N_2O_5 cold trap, NH_4NO_3 particle atomizer + DMA size-selector, or NH_3 permeation tube) is diluted by a zero air flow (with an option for adding O_3, VOCs, RH, or CO through the secondary addition port), and passed through the TD oven. A portion of the flow is sampled prior to entering the oven with one of several type of auxiliary measurement (I- CIMS for N_2O_5, UHSAS for NH_4NO_3 particles, or commercial CRDS for NH_3). After flowing through a cooling region, the sample passes through a particle filter and then is mixed with a ~30 ppmv addition of O_3 in a mixing volume before entering through the optical cavity, where NO_2 is measured by CRDS.

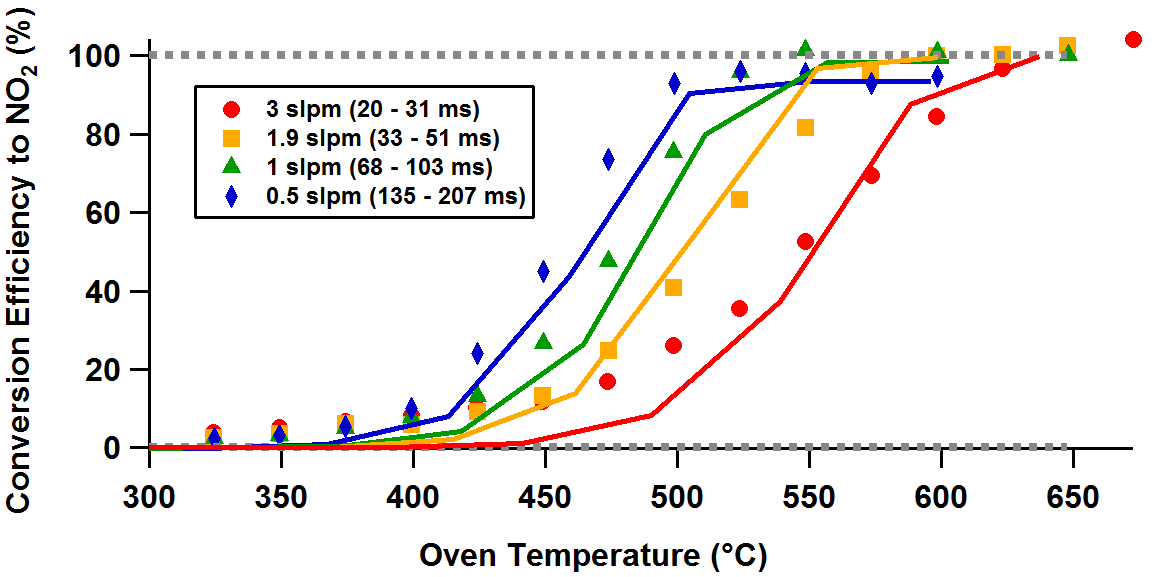

Figure 2. HNO_3 thermograms measured at several flow rates in the NOAA TD-CRDS. Conversion efficiency is calculated as measured NO_2 signal relative to the expected concentration of HNO_3. Parentheses in the legend indicate the range of residence times experienced by the sample in the heated inlet. The grey dashed lines indicate 0 and 100% conversion. Solid lines show simulations using a simple kinetic box model, as described in the text.

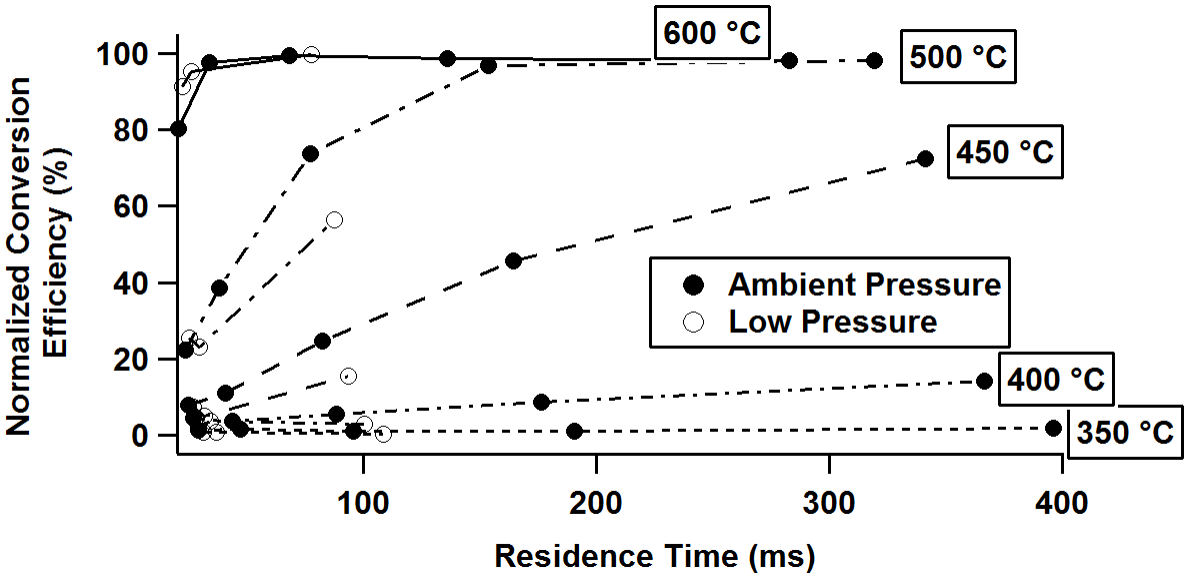

Figure 3. Conversion efficiencies of HNO_3 to NO_2 plotted as a function of plug flow residence times in the oven (see text) for 5 different temperatures. Values were obtained by scaling the measured conversion efficiency in Fig. 1 to the overall maximum and minimum of the thermogram, to account for slight differences between thermograms. Solid circles indicated measurements at ambient pressure, whereas open circles indicate measurements at low pressure. Different line traces indicated different temperatures. A temperature setpoint between 350 (short dashed line) and 450 degrees (long dashed line), and a residence time less than 200 ms are the conditions normally selected for selective detection of alkyl nitrates with no detection of HNO_3. However, under these conditions HNO_3 conversion may be anywhere between 1 and 30%.

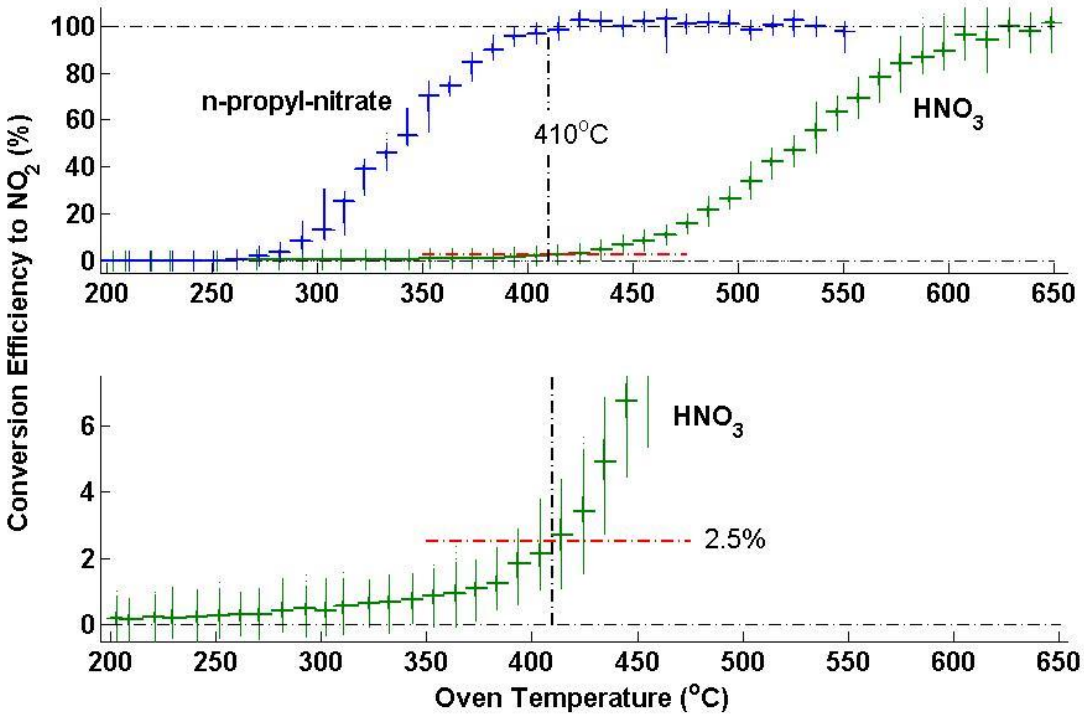

Figure 4. HNO_3 and *n*-propyl-nitrate thermograms taken with the Berkeley TD-LIF instrument used in the NASA DISCOVER-AQ California mission. The lower panel shows only HNO_3 with the y-axis expanded to illustrate the dissociation onset. The oven is from the instrument's alkyl nitrates channel. The flow rate was approximately 2 slpm and the measurement setpoint was 410 ºC. The dataset was corrected for the 2.5% dissociation of HNO_3 in the alkyl nitrates channel. A different oven was used for HNO_3 at a setpoint of 620 ºC.

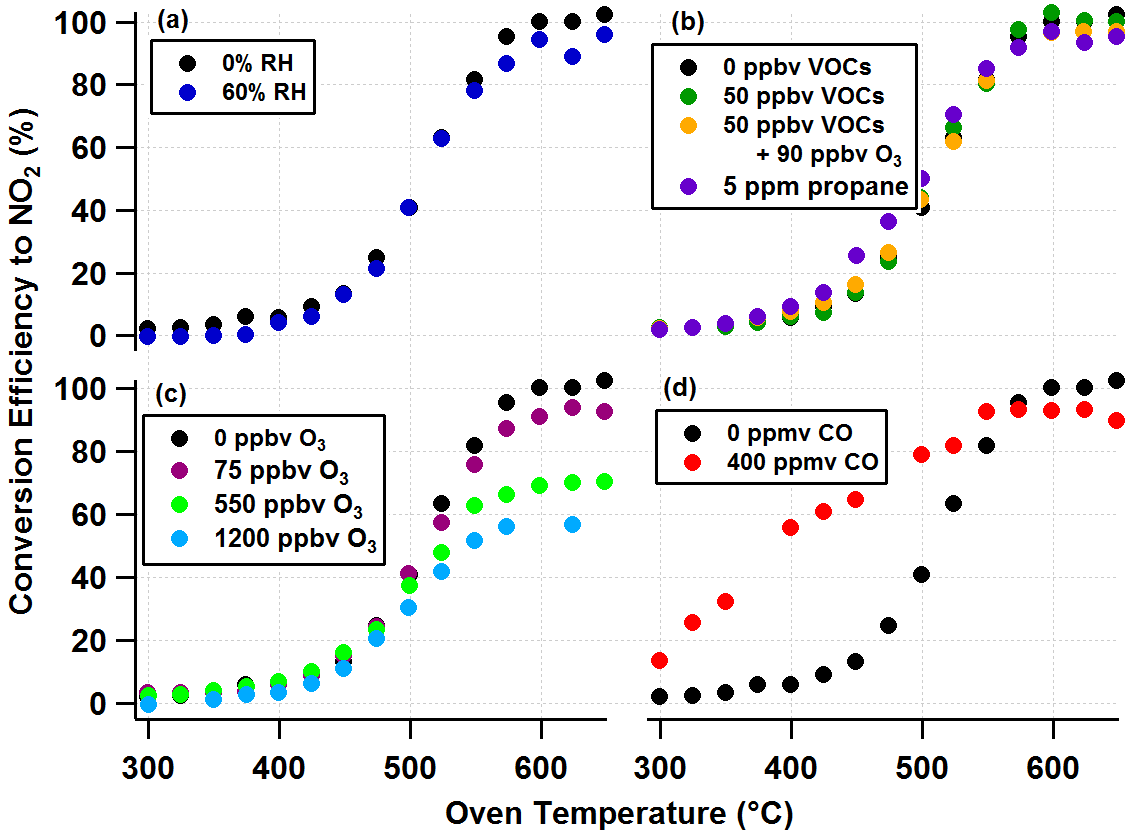

Figure 5. HNO_3 thermograms (1.9 slpm, ambient pressure) taken with the NOAA TD-CRDS, with various additions added prior to the TD oven. In each frame, the black solid circles indicate the no-addition case. In frames (a) and (b): No effect is observed when thermogram is taken at high relative humidity or when VOCs are added. In frame (c), varying amounts of O_3 were added, ranging from ambient levels (75 ppbv) to extremely polluted levels (1200 ppbv), which decreases the overall conversion at high temperatures. In frame (d), the addition of 400 ppmv CO alters the shape of the thermogram.

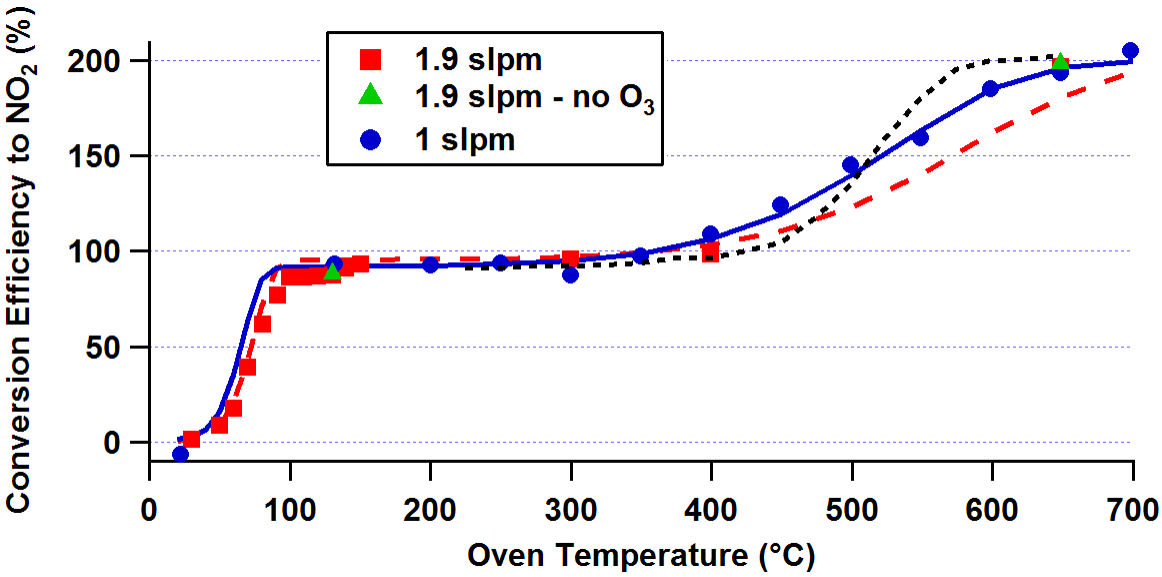

Figure 6. Thermogram of N_2O_5 measured in the NOAA TD-CRDS at two flow rates. The red squares and red dashed line show the 1.9 slpm thermogram and simulation, while the blue circles and blue solid line show the analogous result at 1.0 slpm. The first dissociation corresponds to N_2O_5 → NO_2 + NO_3, and the second to NO_3 → NO_2 + O. The second curve reaches a maximum of 200%, while the first reaches 90 – 95%, depending on the flow rate, due to recombination of NO_2 and NO_3 in the cooling region prior to the detector region. The black dashed line is the experimental HNO_3 thermogram from Fig. 2, offset by 100%. The green triangles indicate measurements of the conversion efficiency without the O_3 addition, confirming that the second dissociation must occur via NO_3 → NO_2 + O rather than NO_3 → NO + O_2.

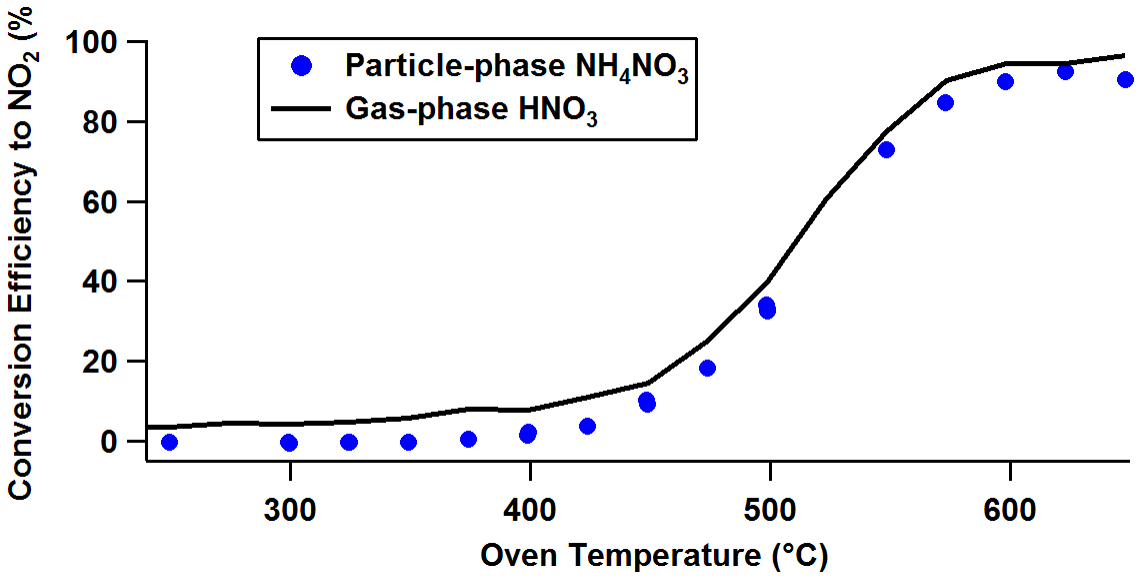

Figure 7. Measured thermogram of NH_4NO_3 particles as solid circles from the NOAA TD-CRDS. The black solid line indicates the measured thermogram of gas-phase HNO_3 at a 1.9 slpm flow rate (from the gold squares trace in Fig. 2). The close match of these two thermograms indicates that the NH_4NO_3 particles go through HNO_3 as an intermediate, and is a good indication that complete conversion is achieved.

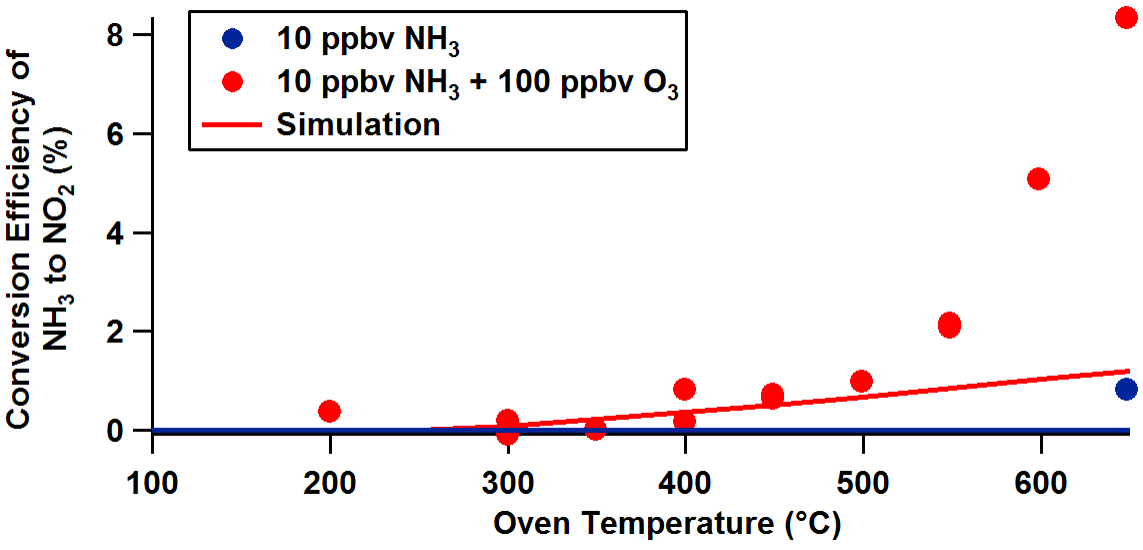

Figure 8. Thermogram of NH_3 taken with the NOAA TD-CRDS, with 100 ppbv of O_3 added before the oven shown as red circles. The blue circle represents an analogous measurement at 650 °C with no O_3 added. Kinetic box model simulations shown in solid lines of corresponding color.

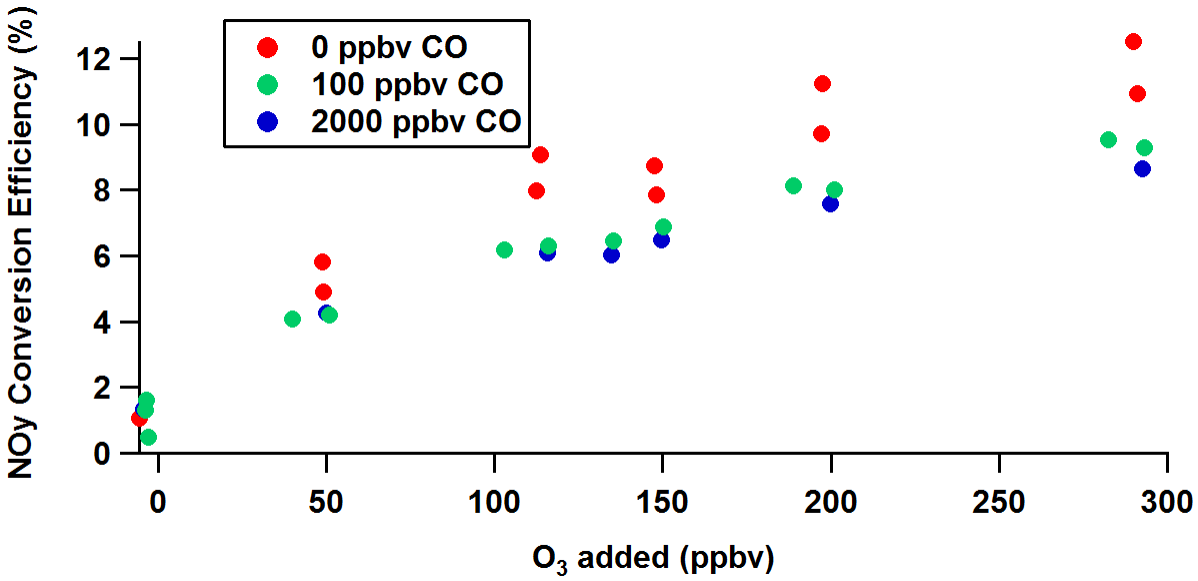

Figure 9. Conversion efficiency of NH_3 to NO_2 as a function of O_3 added to the TD inlet. Red circles show 10 ppbv NH_3 with O_3 ranging from 0 – 300 ppbv, and the green and blue traces show similar data, but with 100 and 2000 ppbv CO added. The partial depletion of the signal (~25%) with the addition of CO indicates that the oxygen atoms formed from O_3 pyrolysis are reacting with CO instead of NH_3.

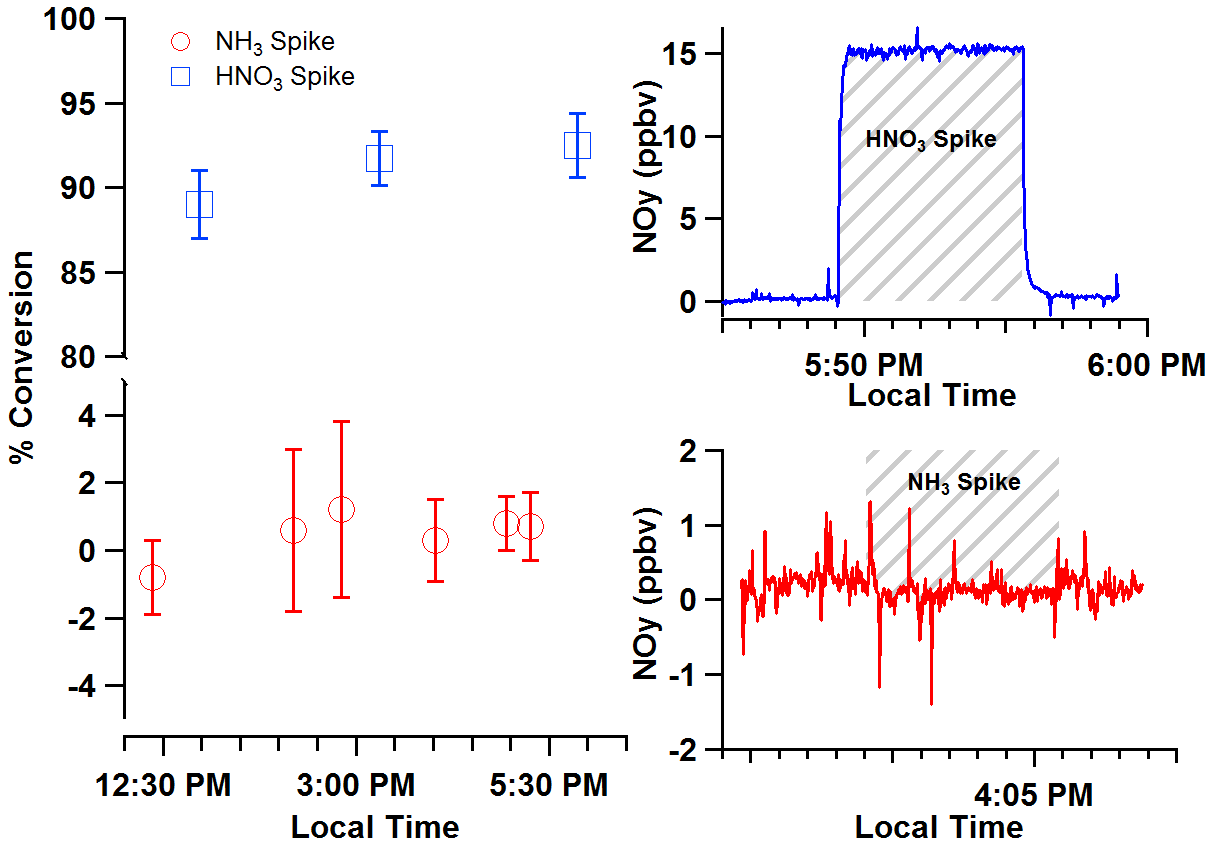

Figure 10. Measurement of HNO_3 and NH_3 conversion in ambient air at an inlet set temperature of 650 °C. The left panel shows measured conversion efficiencies for standard additions of HNO_3 and NH_3 to the NOAA TD-CRDS inlet sampling ambient air in Boulder, CO on August 9, 2016. The right panels show time series of measured NO_y during standard additions. The data is the difference between two NO_y measurement channels, one with and one without the standard addition, to cancel the variation in ambient NO_y during the tests.